Monocyte-derived alveolar macrophages drive lung fibrosis and persist in the lung over the life span

Alexander V. Misharin,[1]* Luisa Morales-Nebreda,[1]* Paul A. Reyfman,[1]* Carla M. Cuda,[2] James M. Walter,[1] Alexandra C. McQuattie-Pimentel,[1] Ching-I Chen,[1] Kishore R. Anekalla,[1] Nikita Joshi,[1] Kinola J.N. Williams,[1] Hiam Abdala-Valencia,[2] Tyrone J. Yacoub,[3] Monica Chi,[1] Stephen Chiu,[1,4] Francisco J. Gonzalez-Gonzalez,[1] Khalilah Gates,[1] Anna P. Lam,[1] Trevor T. Nicholson,[1] Philip J. Homan,[2] Saul Soberanes,[1] Salina Dominguez,[2] Vince K. Morgan,[2] Rana Saber,[2] Alexander Shaffer,[2] Monique Hinchcliff,[2] Stacy A. Marshall,[5] Ankit Bharat,[1,4] Sergejs Berdnikovs,[6] Sangeeta M. Bhorade,[1] Elizabeth T. Bartom,[4] Richard I. Morimoto,[7] William E. Balch,[8] Jacob I. Sznajder,[1] Navdeep S. Chandel,[1] Gökhan M. Mutlu,[9] Manu Jain,[1] Cara J. Gottardi,[1] Benjamin D. Singer,[1] Karen M. Ridge,[1] Neda Bagheri,[2] Ali Shilatifard,[4] G.R. Scott Budinger,[1]** and Harris Perlman[3]**

[1]Division of Pulmonary and Critical Care Medicine, Department of Medicine, Feinberg School of Medicine and [2]Division of Rheumatology, Department of Medicine, Feinberg School of Medicine, Northwestern University, Chicago, IL
[3]Department of Chemical and Biological Engineering, McCormick School of Engineering, Northwestern University, Evanston, IL
[4]Division of Thoracic Surgery, Department of Surgery, Feinberg School of Medicine, [5]Department of Biochemistry and Molecular Genetics, Feinberg School of Medicine, and [6]Division of Allergy and Immunology, Department of Medicine, Feinberg School of Medicine, Northwestern University, Chicago, IL
[7]Department of Molecular Biosciences, Rice Institute for Biomedical Research, Northwestern University, Evanston, IL
[8]Department of Molecular Medicine, The Scripps Research Institutes, La Jolla, CA
[9]Section of Pulmonary and Critical Care Medicine, University of Chicago, Chicago, IL

Little is known about the relative importance of monocyte and tissue-resident macrophages in the development of lung fibrosis. We show that specific genetic deletion of monocyte-derived alveolar macrophages after their recruitment to the lung ameliorated lung fibrosis, whereas tissue-resident alveolar macrophages did not contribute to fibrosis. Using transcriptomic profiling of flow-sorted cells, we found that monocyte to alveolar macrophage differentiation unfolds continuously over the course of fibrosis and its resolution. During the fibrotic phase, monocyte-derived alveolar macrophages differ significantly from tissue-resident alveolar macrophages in their expression of profibrotic genes. A population of monocyte-derived alveolar macrophages persisted in the lung for one year after the resolution of fibrosis, where they became increasingly similar to tissue-resident alveolar macrophages. Human homologues of profibrotic genes expressed by mouse monocyte-derived alveolar macrophages during fibrosis were up-regulated in human alveolar macrophages from fibrotic compared with normal lungs. Our findings suggest that selectively targeting alveolar macrophage differentiation within the lung may ameliorate fibrosis without the adverse consequences associated with global monocyte or tissue-resident alveolar macrophage depletion.

INTRODUCTION

Van Furth and colleagues suggested an adult monocytic origin of all macrophages, but it is now clear that many tissue-resident macrophages, including alveolar macrophages in the lung, are self-renewing populations that arise from fetal progenitors and require minimal input from circuiting adult monocytes in a healthy environment (Guilliams et al., 2013; Yona et al., 2013; Scott et al., 2014; Kopf et al., 2015; van de Laar et al., 2016). In response to macrophage depletion, monocytes are recruited to the lung, where the microenvironment shapes them into cells that closely resemble tissue-resident alveolar macrophages (Landsman and Jung, 2007; Hashimoto et al., 2013; Lavin et al., 2014; Gibbings et al., 2015). Accordingly, during homeostasis, the lung harbors at least one and perhaps two ontologically distinct populations of alveolar macrophages, referred to as tissue-resident alveolar macrophages (TR-AMs) and monocyte-derived alveolar macrophages (Mo-AMs). Our current understanding of the role of alveolar macrophages is almost exclusively based on studies conducted in healthy animals during homeostasis, but

*A.V. Misharin, L. Morales-Nebreda, and P.A. Reyfman contributed equally to this paper.

**G.R.S. Budinger and H. Perlman contributed equally to this paper.

Correspondence to G.R.S. Budinger: s-buding@northwestern.edu; Harris Perlman: h-perlman@northwestern.edu

Abbreviations used: IM, interstitial macrophage; Mo-AM, monocyte-derived alveolar macrophage; PCA, principal-component analysis; RIPK, receptor-interacting protein kinase; RNA-seq, RNA sequencing; TR-AM, tissue-resident alveolar macrophage.

The Rockefeller University Press
J. Exp. Med. 2017 Vol. 214 No. 8 2387–2404
https://doi.org/10.1084/jem.20162152

the differentiation of monocytes into alveolar macrophages may differ in the local microenvironment resulting from tissue injury or fibrosis.

It has long been recognized that depletion of circulating monocytes (e.g., using *Ccr2*$^{-/-}$ mice or via the systemic administration of liposomal clodronate) ameliorates fibrosis severity in the lung and other organs (Moore et al., 2001; Gibbons et al., 2011; Wynn and Vannella, 2016). To explain these findings, investigators have suggested that during injury, monocytes rapidly differentiate into Mo-AMs and that both TR-AMs and Mo-AMs are polarized toward a profibrotic or "M2" phenotype in the fibrotic lung (Zhou et al., 2014). This "macrophage polarization" model is based on limited evidence and is conceptually incomplete (Xue et al., 2014; Nahrendorf and Swirski, 2016). For example, even in the healthy lung, alveolar macrophage differentiation is a slow process that unfolds over a time course longer than most fibrosis models (weeks), raising the possibility that incompletely differentiated alveolar macrophages rather than "polarized" alveolar macrophages contribute to fibrosis (Lavin et al., 2014; Gibbings et al., 2015). Furthermore, the relative contributions of Mo-AMs compared with TR-AMs to the development of fibrosis is not known. Finally, it is not clear whether alveolar macrophages are reconstituted after injury through the differentiation of recruited Mo-AMs or by the proliferation of TR-AMs and, if the former, whether these ontologically distinct populations are functionally different. Answers to these questions are important for the design of monocyte/macrophage–targeted therapies. In particular, monocyte-depletion strategies are limited by the requirement for a continuous supply of monocyte-derived cells for homeostasis in the gut and other tissues; therefore, it is critical to know whether selectively targeting Mo-AMs after they have lost canonical monocyte markers can ameliorate fibrosis. Similarly, strategies that nonselectively deplete both TR-AMs and Mo-AMs might paradoxically worsen fibrosis by inducing further recruitment of monocytes and threaten tissue homeostasis through the loss of TR-AM function (Janssen et al., 2011; Gibbings et al., 2015).

To address these questions, we developed a novel lineage tracing system in mice to unambiguously identify Mo-AMs and TR-AMs during the development of fibrosis and over the subsequent life span of the animal. We used this system to show that lung fibrosis was ameliorated when Mo-AMs were driven to necroptosis during their differentiation without affecting monocytes, thereby establishing a causal link between Mo-AMs and the pathobiology of fibrosis. In contrast, depletion of TR-AMs before the induction of lung fibrosis did not alter fibrosis severity. In 14-mo-old untreated mice, >95% of AMs were TR-AMs, but in mice treated with bleomycin at 4 mo of age, the alveolar macrophage pool was comprised of both TR-AMs and Mo-AMs, suggesting that a subpopulation of Mo-AMs persists after the resolution of fibrosis. Using transcriptomic profiling of monocyte-derived populations collected over the course of fibrosis and its resolution, we show that monocyte to macrophage differentiation unfolds slowly over weeks. Genes identified by others as causally linked to the development of fibrosis were most highly expressed in Mo-AMs early during their differentiation and were progressively down-regulated as Mo-AMs differentiated into mature alveolar macrophages. TR-AMs and Mo-AMs showed significant differences in profibrotic gene expression during fibrosis; however, 10 mo after the injury, these differences were no longer evident. Human homologues of many of the profibrotic genes expressed in Mo-AMs during bleomycin-induced fibrosis were differentially expressed in flow-sorted alveolar macrophages obtained from the lungs of patients with fibrotic lung disease. These results reveal remarkable heterogeneity in alveolar macrophage function during lung fibrosis with important implications for the design of targeted therapy.

RESULTS

In the absence of tissue injury, monocyte to macrophage differentiation is thought to be regulated by epigenetic changes in response to factors present in the lung microenvironment (Lavin et al., 2014). Depletion of circulating monocytes using *Ccr2*$^{-/-}$ mice or the administration of liposomal clodronate reduces fibrosis severity, implicating monocyte-derived cells in the development of fibrosis (Moore et al., 2001; Gautier et al., 2012; Lavin et al., 2014; Gibbings et al., 2015). However, we know little about the importance of monocytes or monocyte-derived cells after they leave the circulation. We have previously shown that 5 d after administration of bleomycin, the number of interstitial macrophages (identified as CD64^{+}Silgec F^{-}) was increased, whereas the number of alveolar macrophages (CD64^{+}Siglec F^{+}) was reduced. In contrast, during the fibrotic phase (day 21 post–bleomycin administration), the number of interstitial macrophages decreased and the number of alveolar macrophages increased because of the appearance of alveolar macrophages characterized by lower expression of Siglec F (Siglec F^{low}; Fig. 1, A and B; Misharin et al., 2013). To determine whether this new population of cells represented an expansion of TR-AMs or the recruitment of Mo-AMs, we developed a lineage tracing system that allows us to distinguish alveolar macrophage ontogeny during injury and over the subsequent life span of the animal (Fig. 1 C). Using this system, we showed that the increase in alveolar macrophages during fibrosis was completely attributable to monocyte-derived cells (i.e., Mo-AMs). Furthermore we found that differential expression of Siglec F reliably distinguished Mo-AMs and TR-AMs over the course of bleomycin-induced fibrosis (Fig. 1, B, E, and F; Misharin et al., 2013), and we used this gating strategy (Fig. S1) to identify TR-AMs and Mo-AMs in subsequent studies.

We next sought to determine whether Mo-AMs, TR-AMs, or both contributed to the development of fibrosis. First, to target Mo-AMs, we used mice with targeted depletion of capsase-8 in macrophages (Cuda et al., 2014, 2015). Caspase-8 is a cysteine protease that serves the dual function

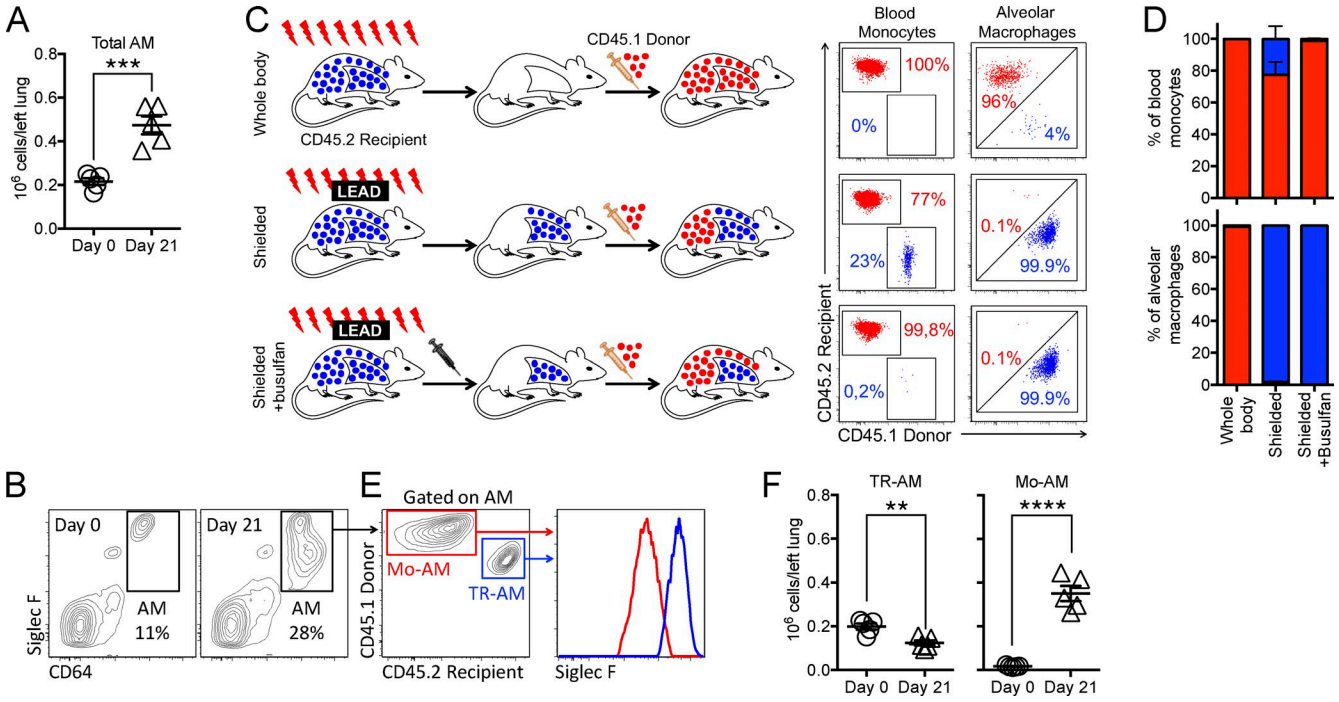

Figure 1. **TR-AMs are depleted during lung fibrosis and replaced with Mo-AMs.** (A and B) The alveolar macrophage pool is expanded 21 d after the intratracheal administration of bleomycin when fibrosis is maximal because of the appearance of a novel population of cells characterized by lower expression of Siglec F (n = 5 per group, paired t test; data are shown as mean ± SEM; ***, P < 0.001). (C) Schematic explaining the technique for the generation of bone marrow chimeras with thoracic shielding and busulfan and representative dot plots reflecting chimerism in peripheral blood monocytes and alveolar macrophages in the lung 8 wk after irradiation and bone marrow transfer. Whole-body irradiation leads to complete replacement of recipient monocytes and alveolar macrophages with donor-derived cells (top). Irradiation with thoracic shielding protects alveolar macrophages but results in incomplete chimerism among circulating monocytes (middle). The addition of busulfan conditioning postirradiation allows complete elimination of recipient's monocytes while preserving alveolar macrophages (bottom). (D) Percentage of monocytes and alveolar macrophages of donor and recipient origin 8 wk after the generation of chimeras (n = 3–5 per group; data are shown as mean ± SEM and are representative of >100 mice). (E) The new population of alveolar macrophages that emerges during bleomycin-induced fibrosis ($CD45^+CD11b^{+/-}CD11c^+CD64^+SiglecF^{low}$) is monocyte derived. Representative contour plots show expansion of the alveolar macrophage pool; numbers indicate percentage of the parent population (gated on singlets/live/$CD45^+$ cells). (F) Expansion of the alveolar macrophage pool during bleomycin-induced lung fibrosis is caused by recruitment of Mo-AMs, whereas the number of TR-AMs is decreased (n = 5 per group, paired t test; data are shown as mean ± SEM and are representative of more than five independent experiments; **, P < 0.01; ****, P < 0.0001).

of activating the extrinsic apoptotic pathway in response to death ligands and suppressing receptor-interacting protein kinase (RIPK)–mediated necroptosis during development and inflammation (Lu et al., 2014; Salvesen and Walsh, 2014). We deleted *Casp8* from different monocyte/macrophage populations using two independent Cre drivers ($CD11c^{Cre}Casp8^{flox/flox}$ and $LysM^{Cre}Casp8^{flox/flox}$) that both efficiently target alveolar macrophages. We then administered intratracheal bleomycin to $Casp8^{flox/flox}$, $CD11c^{Cre}Casp8^{flox/flox}$, and $LysM^{Cre}Casp8^{flox/flox}$ mice and compared the severity of fibrosis after 21 d. We found that although a substantial fraction of control $Casp8^{flox/flox}$ mice died in response to bleomycin, survival was improved in both $CD11c^{Cre}Casp8^{flox/flox}$ and $LysM^{Cre}Casp8^{flox/flox}$ animals (Fig. 2 A). Furthermore, the severity of fibrosis was significantly worse in $Casp8^{flox/flox}$ animals than in $CD11c^{Cre}Casp8^{flox/flox}$ and $LysM^{Cre}Casp8^{flox/flox}$ animals (Fig. 2, B–D). We confirmed these results in another model of lung fibrosis induced by the intratracheal administration of an adenoviral vector encoding an active form of TGF-β (Lam et al., 2014; Morales-Nebreda et al., 2015). Mice with macrophage-targeted deletion of *Casp8* showed attenuated Ad-TGF-β–induced fibrosis (Fig. S2, A–C). One model for alveolar macrophage development involves the sequential differentiation of monocytes into interstitial macrophages (IMs), which in turn differentiate into alveolar macrophages, although it is also possible that monocytes differentiate directly into alveolar macrophages. We observed reduced numbers of Mo-AMs and increased numbers of IMs in $CD11c^{Cre}Casp8^{flox/flox}$ and $LysM^{Cre}Casp8^{flox/flox}$ animals when compared with $Casp8^{flox/flox}$ animals (Fig. 2, E and F; and Fig. S2, D and E), suggesting that Mo-AMs are lost during the differentiation of IMs or monocytes.

Our findings could be explained by the induction of necroptosis in Mo-AMs as they differentiate in the lungs of *Casp8*-deficient mice during fibrosis. If so, we reasoned that deletion of RIPK3 in $CD11c^{Cre}Casp8^{flox/flox}$ and $LysM^{Cre}$

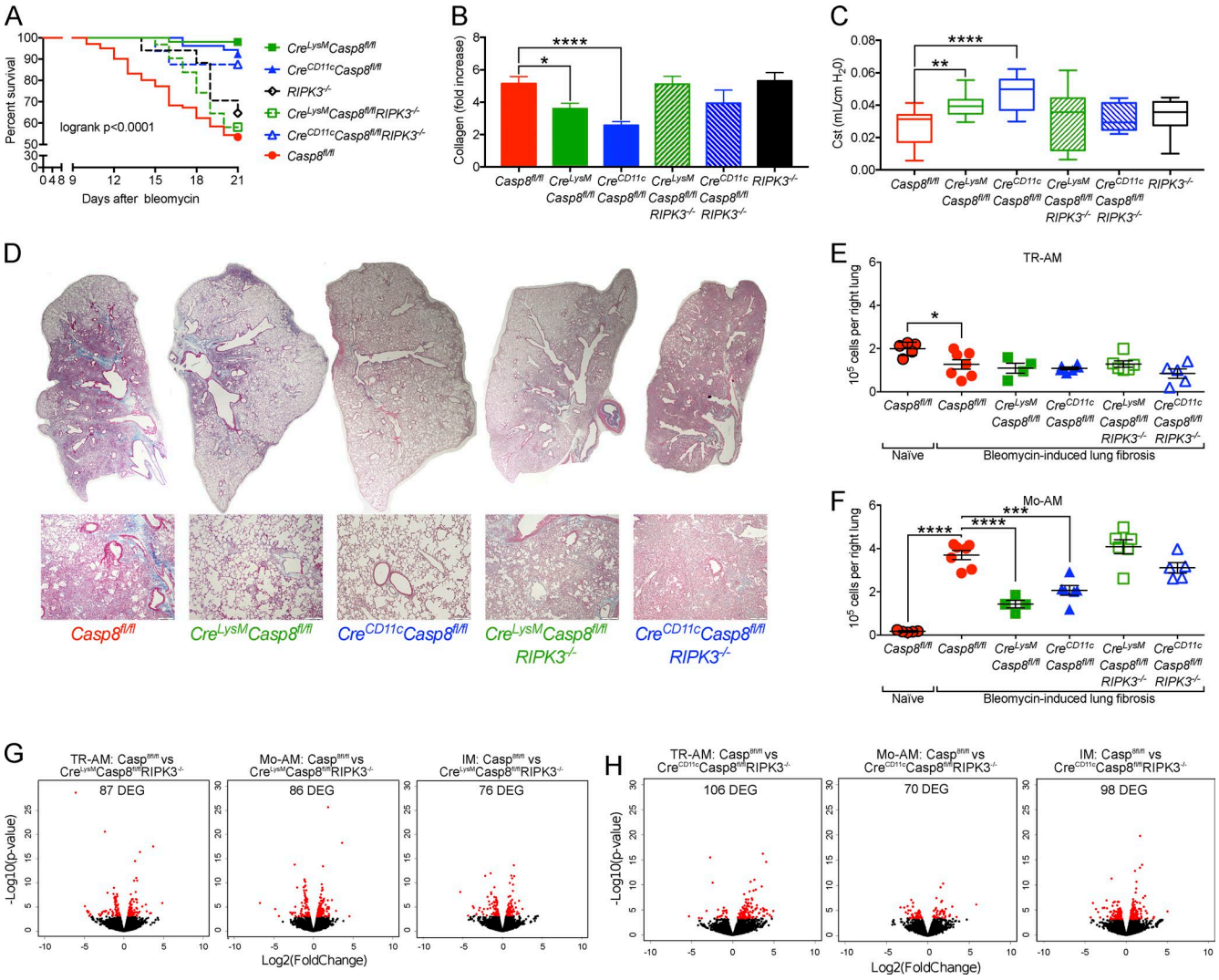

Figure 2. **Necroptosis of Mo-AMs attenuates bleomycin-induced lung fibrosis.** (A–D) Mice with deficiency of *Casp8* in alveolar macrophages have (A) improved survival (16–101 mice per group; combined data from 10 independent experiments; Mantel-Cox log-rank test), (B) lower levels of collagen, (C) improved static lung compliance, and (D) less extent histological fibrosis compared with controls, whereas simultaneous deletion of RIPK3 rescues bleomycin-induced lung fibrosis in $CD11c^{Cre}Casp8^{flox/flox}$ and $LysM^{Cre}Casp8^{flox/flox}$ mice (n = 9–45 mice per group, data expressed as mean ± SEM, one-way ANOVA with Dunnett's test for multiple comparisons; *, P < 0.05; **, P < 0.01; ****, P < 0.0001). (E and F) Protection from lung fibrosis is associated with the loss of Mo-AMs, but not TR-AMs, in *Casp8*-deficient mice, whereas *RIPK3* deficiency rescues Mo-AMs (n = 4–5 mice per group; data are expressed as mean ± SEM; one-way ANOVA with Dunnett's test for multiple comparisons; *, P < 0.05; ***, P < 0.001; ****, P < 0.0001; the experiment was performed at least two times). (G and H) The loss of *RIPK3* does not alter the response of alveolar or interstitial macrophages to fibrosis in $CD11c^{Cre}Casp8^{flox/flox}RIPK3^{-/-}$ and $LysM^{Cre}Casp8^{flox/flox}RIPK3^{-/-}$ mice. Volcano plot showing number of differentially expressed genes (red, FDR q value < 0.05; n = 2–5 mice per group). DEG, differentially expressed genes.

$Casp8^{flox/flox}$ animals should restore the Mo-AM population and "rescue" fibrosis. To test this hypothesis, we generated $Casp8^{flox/flox}$, $CD11c^{Cre}Casp8^{flox/flox}RIPK3^{-/-}$, and $LysM^{Cre}Casp8^{flox/flox}RIPK3^{-/-}$ mice and treated them with bleomycin. The loss of RIPK3 restored the population of Mo-AMs to control levels, and the severity of fibrosis in $Casp8^{flox/flox}$, $CD11c^{Cre}Casp8^{flox/flox}RIPK3^{-/-}$, and $LysM^{Cre}Casp8^{flox/flox}RIPK3^{-/-}$ mice was similar to that seen in $Casp8^{flox/flox}$ animals (Fig. 2, A–F). These data suggest that RIPK3 is activated during monocyte to macrophage differentiation. To exclude a functional role for RIPK3 in alveolar macrophage differentiation, as has been suggested in bone marrow–derived cells (Dannappel et al., 2014; Moriwaki et al., 2014; Vlantis et al., 2016), we flow-sorted Mo-AMs from $Casp8^{flox/flox}$, $CD11c^{Cre}Casp8^{flox/flox}RIPK3^{-/-}$, and $LysM^{Cre}Casp8^{flox/flox}RIPK3^{-/-}$ mice and measured their transcriptomes using RNA sequencing (RNA-seq). We found that only a small number of genes were differentially expressed

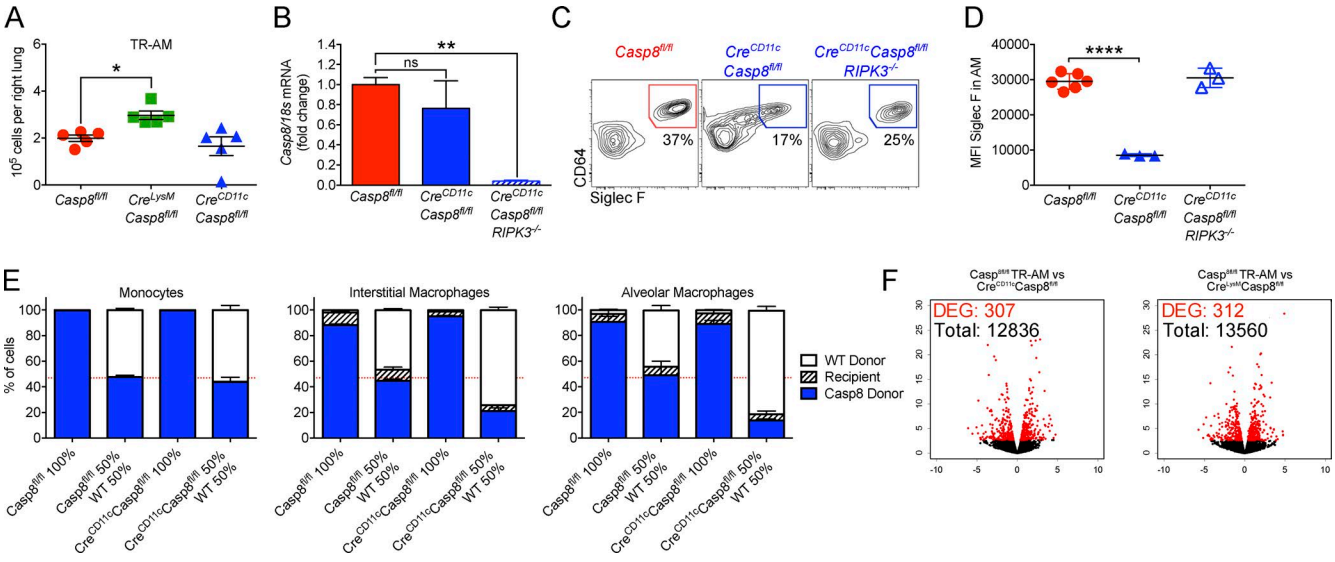

Figure 3. **TR-AMs in *LysM*^{Cre}*Casp8*$^{flox/flox}$ and *CD11c*^{Cre}*Casp8*$^{flox/flox}$ mice have preserved expression of *Casp8*, suggesting they escape Cre-mediated recombination.** (A) *CD11c*^{Cre}*Casp8*$^{flox/flox}$ and *LysM*^{Cre}*Casp8*$^{flox/flox}$ mice have a normal number of TR-AMs in a steady state (n = 5 mice per group; data are shown as mean ± SEM; one-way ANOVA with Dunnett's test for multiple comparisons; *, P < 0.05; the experiment was performed three times). (B) *Casp8* expression in flow-sorted TR-AMs measured by quantitative PCR (n = 3–5 mice per group; data are shown as mean ± SEM; one-way ANOVA with Dunnett's test for multiple comparisons; **, P < 0.01; the experiment was performed two times). (C and D) Bone marrow from *CD11c*^{Cre}*Casp8*$^{flox/flox}$ mice fails to reconstitute the alveolar niche 8 wk after irradiation, as indicated by ongoing recruitment of the immature Mo-AMs with low expression of Siglec F. Repopulation of the alveolar niche was rescued in *CD11c*^{Cre}*Casp8*$^{flox/flox}$*RIPK3*$^{-/-}$ mice (n = 4–5 mice per group; data are expressed as mean ± SEM; one-way ANOVA with Dunnett's test for multiple comparisons; ****, P < 0.0001). (E) Alveolar macrophages derived from bone marrow from *CD11c*^{Cre}*Casp8*$^{flox/flox}$ mice fail to reconstitute the alveolar niche 8 wk after irradiation, as shown by decreased expression of Siglec F on alveolar macrophages. Mice were lethally irradiated, followed by reconstitution with bone marrow from control mice (*Casp8*$^{flox/flox}$) or bone marrow from mice with deletion of *Casp8* in cells expressing *CD11c* (*Cre*^{CD11c}*Casp8*$^{flox/flox}$), either alone or in combination with bone marrow from wild-type mice (50% mixture of the two genotypes). Monocytes, interstitial macrophages, and alveolar macrophages were identified by flow cytometry of lung homogenates 8 wk later (CD45.1 or CD45.2 mice were used for lineage tracing). Although ∼50% of monocytes in both *Casp8*$^{flox/flox}$ and *Cre*^{CD11c}*Casp8*$^{flox/flox}$ mice were wild-type cells, the majority of interstitial macrophages and alveolar macrophages in mice reconstituted with *Cre*^{CD11c}*Casp8*$^{flox/flox}$ bone marrow, but not *Casp8*$^{flox/flox}$ mice, were of wild-type origin, suggesting the loss of *Casp8* during differentiation results in a selective disadvantage in the differentiation of monocytes in to alveolar macrophages; data are shown as mean ± SEM. (F) Cells that escaped Cre-mediated recombination behave similarly to wild-type cells during fibrosis (day 14) with <1% differentially expressed genes (DEG). Volcano plot showing number of differentially expressed genes (red, FDR q value <0.05, n = 2–5 mice per group).

in all investigated cell types, suggesting RIPK activation is largely dispensable for alveolar macrophage differentiation and fibrosis in this model (Fig. 2, G and H).

Both *Cre*^{LysM} and *Cre*^{CD11c} should effectively target both Mo-AMs and TR-AMs; therefore, we wondered whether the protection we observed in the *CD11c*^{Cre}*Casp8*$^{flox/flox}$ and *LysM*^{Cre}*Casp8*$^{flox/flox}$ mice be partially attributed to deletion of *Casp8* in TR-AMs. Both *CD11c*^{Cre}*Casp8*$^{flox/flox}$ and *LysM*^{Cre}*Casp8*$^{flox/flox}$ mice had normal numbers of TR-AMs in comparison to *Casp8*$^{flox/flox}$ mice (Fig. 3 A). Surprisingly, the levels of *Casp8* mRNA in TR-AMs from naive *CD11c*^{Cre} *Casp8*$^{flox/flox}$ mice were similar to those in the *Casp8*$^{flox/flox}$ mice (Fig. 3 B). This suggested to us that RIPK-mediated necroptosis might occur as fetal monocytes differentiate into TR-AMs during the early postnatal period, thereby providing a selection pressure favoring TR-AMs that escape recombination. Consistent with this hypothesis, *Casp8* was efficiently deleted in TR-AMs from the *RIPK3*$^{-/-}$ animals (Fig. 3 B). To confirm that the loss of *Casp8* prevented the differentiation of monocytes into Mo-AMs, we compared the ability of bone marrow from *Casp8*-deficient donors to reconstitute the alveolar macrophage pool in the presence or absence of RIPK3. Compared with wild-type bone marrow, bone marrow from the *Casp8*-deficient donors on a wild-type background inefficiently repopulated the alveolar macrophage pool, as shown by ongoing recruitment of alveolar macrophages with low levels of Siglec F expression in *CD11c*^{Cre}*Casp8*$^{flox/flox}$ relative to *Casp8*$^{flox/flox}$ mice (Fig. 3, C and D). Deletion of RIPK3 (*CD11c*^{Cre}*Casp8*$^{flox/flox}$*RIPK3*$^{-/-}$) restored the monocyte to alveolar macrophage differentiation, as indicated by normal levels of Siglec F. We confirmed these findings by demonstrating a reduced ability of bone marrow from *CD11c*^{Cre} *Casp8*$^{flox/flox}$ relative to *Casp8*$^{flox/flox}$ mice to reconstitute the alveolar macrophage, but not circulating monocyte, pool in 1:1 completive chimera experiments (Fig. 3 E).

To exclude the possibility that the partial loss of *Casp8* we observed in TR-AMs from *CD11c*^{Cre}*Casp8*$^{flox/flox}$ and *LysM*^{Cre}*Casp8*$^{flox/flox}$ relative to *Casp8*$^{flox/flox}$ mice might ac-

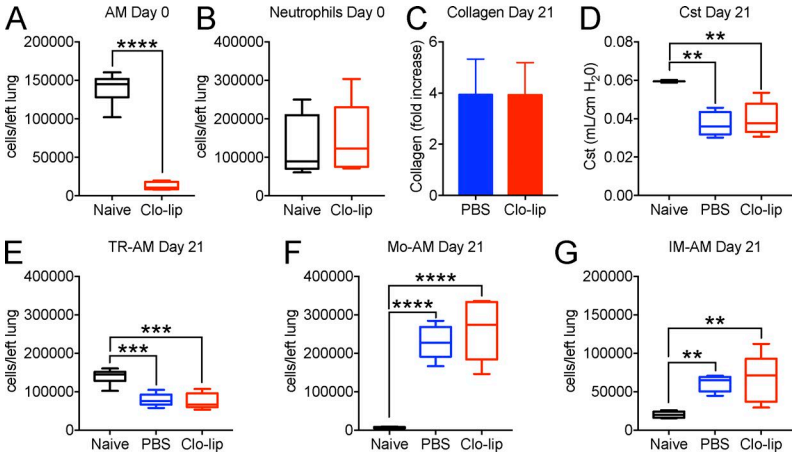

Figure 4. **Depletion of TR-AMs does not protect from bleomycin-induced lung fibrosis.** (A and B) Intratracheal administration of 50 µl clodronate-loaded liposomes (Clo-lip) results in nearly complete depletion of TR-AMs 3 d later without recruitment of neutrophils. (C and D) Mice with depleted TR-AMs showed the same severity of bleomycin-induced lung fibrosis, as indicated by collagen levels (C) and static lung compliance (D) 21 d later. (E–G) Numbers of TR-AMs (E), Mo-AMs (F), and interstitial macrophages (IMs; G) did not differ between the clodronate-loaded liposome–treated and control (PBS) groups (n = 5–6 mice per group; data are expressed as mean ± SEM; one-way ANOVA with Dunnett's test for multiple comparisons; **, $P < 0.01$; ***, $P < 0.001$; ****, $P < 0.0001$; the experiment was performed one time).

count for the protection these mice exhibited against bleomycin-induced fibrosis, we compared the transcriptomes of sorted naive TR-AMs from *Casp8*$^{flox/flox}$, *CD11c*^{Cre}*Casp8*$^{flox/flox}$ and *LysM*^{Cre}*Casp8*$^{flox/flox}$ mice during fibrosis (day 14) and found that <1% of transcripts were differentially expressed (Fig. 3 F), suggesting that the protection we observed in *CD11c*^{Cre}*Casp8*$^{flox/flox}$ and *LysM*^{Cre}*Casp8*$^{flox/flox}$ mice against fibrosis was attributable to the loss of Mo-AMs. To exclude the possibility that TR-AMs also contribute to the development of fibrosis, we selectively depleted TR-AMs by administering liposomal clodronate intratracheally 3 d before the administration of bleomycin. The administration of liposomal clodronate effectively depleted TR-AMs without inducing the recruitment of neutrophils (Fig. 4, A and B). Although TR-AMs were reduced in intratracheal liposomal clodronate–treated animals over the course of bleomycin-induced fibrosis, there was no difference in the recruitment of Mo-AM, interstitial macrophages or in the severity of fibrosis (Fig. 4, C–G), suggesting TR-AMs do not contribute to the development of fibrosis in this model.

Our data suggest that Mo-AMs contribute disproportionately to the development of lung fibrosis. To better understand the function of these cells during lung fibrosis, we flow-sorted monocytes, interstitial macrophages, Mo-AMs, and TR-AMs 14 and 19 d after the administration of bleomycin and analyzed their gene expression using RNA-seq (Fig. 5 A). Principal-component analysis (PCA) of the differentially expressed genes showed clustering of the replicates according to cellular populations, suggesting that flow cytometry identifies differences in cellular phenotypes that can be reproducibly detected at the level of the transcriptome (Fig. 5 B; Fig. S3, A and B; and Table S1). We then performed k-means clustering of the entire transcriptional dataset (12,968 genes), which revealed five distinct clusters of genes (Fig. 5 C, Fig. S3 C, and Tables S2 and S3). Clusters I and II contained core gene signatures that were progressively up-regulated and down-regulated during monocyte to alveolar macrophage differentiation, respectively. Genes in these clusters were similar to those others have associated with monocyte to alveolar macrophage differentiation during homeostasis (Fig. S3 G; Lavin et al., 2014; Schneider et al., 2014). Genes in clusters IV and V were up-regulated early and late during fibrosis, respectively. Early genes (cluster IV) included those involved in biosynthetic pathways, whereas later genes (cluster V) included those involved in epigenetic regulation of gene expression, consistent with the described epigenetic regulation of alveolar macrophage differentiation in the lung (Lavin et al., 2014). These data show that monocyte to alveolar macrophage differentiation unfolds slowly over the course of fibrosis.

Because Mo-AMs substantially outnumber TR-AMs during the development of fibrosis, it is possible that both populations respond to fibrosis similarly, but Mo-AMs predominate numerically. To address this question, we compared the expression of profibrotic genes in Mo-AMs and TR-AMs during the development of fibrosis. Cluster III included genes and pathways that are not known to be expressed in alveolar macrophages during homeostasis, are not associated with processes involved in cellular differentiation, and are associated with fibrosis (Fig. 5 C). These genes were differentially expressed in monocyte-derived cells (interstitial macrophages and Mo-AMs compared with TR-AMs). We performed pairwise comparisons of Mo-AMs, interstitial macrophages, and TR-AMs collected 14 or 19 d after bleomycin with naive TR-AMs (Fig. 6 A and Fig. S4 A). 14 d after the administration of bleomycin, we identified 3,232 genes differentially expressed between TR-AMs and naive TR-AMs and 5,039 genes differentially expressed between Mo-AMs and naive TR-AMs (FDR $P < 0.05$; Fig. 6 A). Functionally similar genes were differentially expressed 19 d after the administration of bleomycin, but the number of differentially expressed genes was smaller (Fig. S4 A). Gene ontology analysis of the differentially expressed genes revealed pathways involved in cell adhesion, cell migration, and fibrosis (Fig. 6, B and C; and Fig. S4 B). Indeed, of the 387 genes in cluster III that were differentially expressed in Mo-AMs compared with TR-AMs, 130 were linked to fibrosis in PubMed (Fig. 6 D). For 29 of the genes, other groups have reported that mice lacking the gene

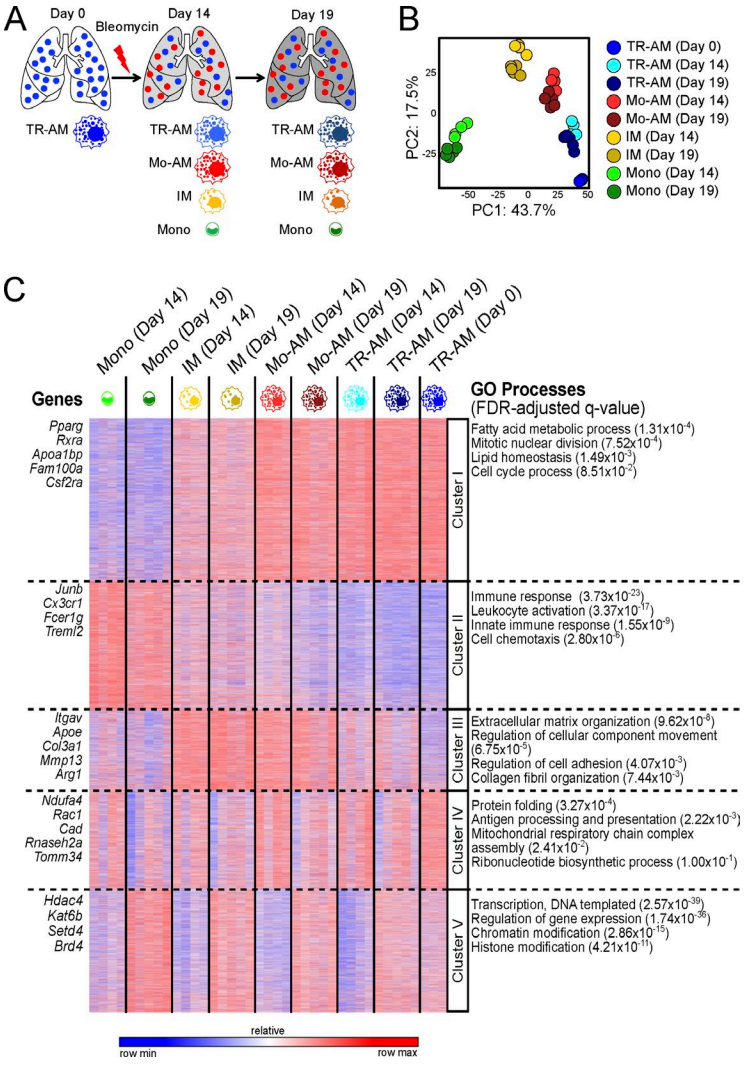

Figure 5. **TR-AMs and Mo-AMs differ in their response to bleomycin-induced lung fibrosis.** (A–C) Transcriptional profiling of macrophage populations over the course of bleomycin-induced lung fibrosis. (A) Experimental outline. (B) Principal-component analysis (PCA) of the transcriptomes of FACS-sorted monocytes, interstitial macrophages (IM), Mo-AMs, and TR-AMs during the course of bleomycin-induced lung fibrosis shows that a significant fraction of the variance in the dataset can be explained by principal component 1 (PC1; 43.7%, differentiation) and principal component 2 (PC2; 17.5%, fibrosis time course). PCA was performed on differentially expressed genes identified from a generalized linear model to perform an ANOVA-like test for differential expression between any conditions in the dataset (FDR step-up procedure q-value < 0.05). (C) k-means clustering of all identified genes revealed clusters of genes associated with monocyte into alveolar macrophage differentiation (clusters I and II), genes differentially expressed over the course of bleomycin-induced lung fibrosis (clusters IV and V), and genes specifically up-regulated in IM and Mo-AMs, but not in monocytes or TR-AMs (cluster III; optimal k of 5 determined from within-group and between-group sum of squares analysis; Fig. S3 C). The characteristic genes and GO processes associated with each cluster are shown on the left and the right sides, correspondingly (see Table S3).

were protected against fibrosis in mouse models, including lung (Moore et al., 2006; Flechsig et al., 2010; Riteau et al., 2010; Aschner et al., 2014; Shibata et al., 2014; Tan et al., 2014; Vuga et al., 2014; Agassandian et al., 2015; Brodeur et al., 2015; Wang et al., 2015; Lv et al., 2016), heart (Li et al., 2009; Fan et al., 2014; Nishikido et al., 2016; Toba et al., 2016), liver (Seki et al., 2009; Kim et al., 2010; Madala et al., 2010; Fiorotto et al., 2016; Marí et al., 2016), kidney (Grgic et al., 2009; Lai et al., 2014; Yan et al., 2016), bone (Ishizuka et al., 2011), eye (Chan et al., 2013), muscle (Sinadinos et al., 2015), and skin (Wang et al., 2015). Genes exclusively expressed in TR-AMs included those involved in lipid metabolic processes and blood microparticle formation (Fig. 6 B). We performed a functional network analysis of the top 100 differentially expressed genes in cluster III using DAVID and Fgnet tools (Fontanillo et al., 2011; Aibar et al., 2015). This analysis revealed 14 highly overlapping metagroups with a core set of hub genes implicated in fibrotic signaling processes (e.g., *Adam8*, *Arg1*, *Apoe*, *Itga6*, *Mfge8*, *Mmp12*, *Mmp13*, *Mmp14*, and *Pdgfa*; Fig. 6 E and Table S4).

Macrophage polarization refers to distinct sets of inflammatory (M1) or fibrotic (M2) genes that are expressed by macrophages in cell culture that are first induced toward differentiation and then treated with LPS and IFN-γ or IL-4, respectively (Martinez and Gordon, 2014; Murray et al., 2014). It has been suggested that polarization of alveolar macrophages toward a profibrotic or "M2" phenotype contributes to the development of fibrosis (Murray et al., 2010; Larson-Casey et al., 2016). Our transcriptional data allowed us to directly test this hypothesis by examining the expression of 20 "M1" and 44 M2 genes during bleomycin-induced lung fibrosis (Misharin et al., 2014). Interestingly, we found that both Mo-AMs and TR-AMs up-regulated M1 and M2 genes in response to bleomycin without a discernible shift in gene expression toward a M1 or M2 phenotype in either cell population. When compared with naive TR-AMs, 25% of M1 genes and 18% of M2 genes were differentially higher in interstitial macrophages and Mo-AMs during fibrosis (Fig. 6 F and Fig. S4 C). In addition, many M2 genes were higher in naive

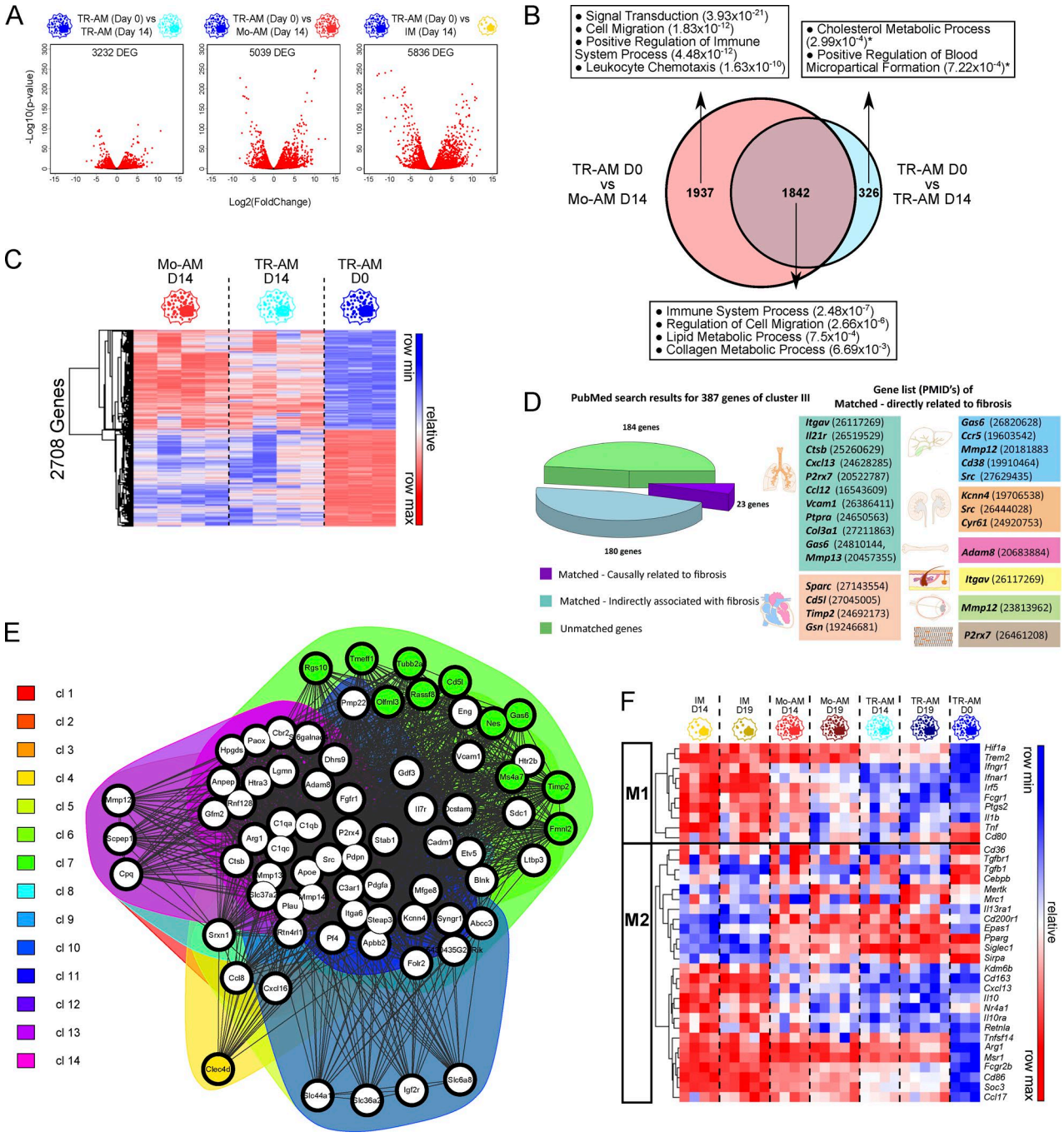

Figure 6. **Monocyte-derived and tissue-resident alveolar macrophages differ in their response to bleomycin-induced lung injury.** (A) Volcano plots demonstrating the number of differentially expressed genes (DEG) for the selected comparisons 14 d after instillation of bleomycin (FDR step-up procedure q-value < 0.05). (B) Comparison of DEG and associated GO processes reveals shared and unique response between Mo-AMs and TR-AMs. (C) Hierarchical clustering of the 2708 DEG shared by Mo-AMs and TR-AMs during the response to bleomycin-induced lung fibrosis. (D) Association between genes in cluster III and fibrosis. Differentially expressed genes from cluster III were taken; term "AND Fibrosis" was added to the gene names and the resulting term was used as input term in the PubMed search engine to search abstracts and full text using an in-house Python script. The abstracts were then manually reviewed for evidence of a genetic association with fibrosis (gene knockouts were protected from fibrosis or transgenic overexpression of the gene increased fibrosis). Of the 387 differentially expressed genes in cluster III (FDR q-value < 0.05), 203 were linked with fibrosis in PubMed and 23 were causally related to the development of fibrosis in different organs (as indicated by images in figure) in genetic mouse models. The numbers in parenthesis are PubMed IDs. (E) Functional gene network analysis was performed on the top 100 of differentially expressed genes between Mo-AMs and TR-AMs from cluster III using GeneTerm Linker and visualized using FGNet tool. White circles indicate hub genes that belong to the multiple metagroups. For metagroup annotations, see Table S4. (F) Heat map of M1/M2 genes that were differentially expressed in our dataset (FDR step-up q-value < 0.05; see also Fig. S4 C).

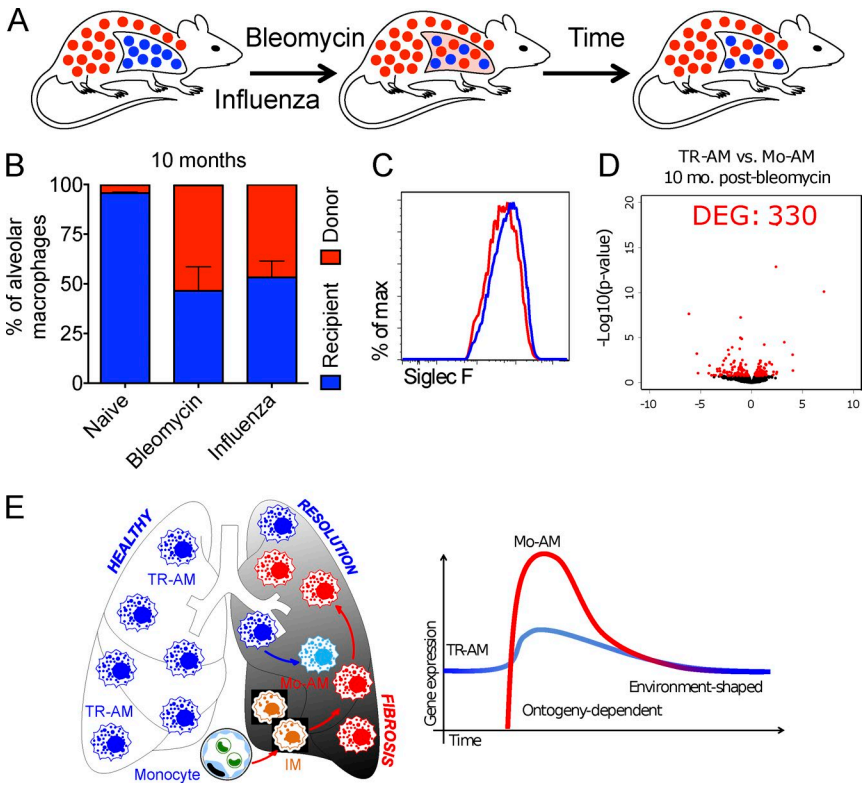

Figure 7. **Monocyte-derived alveolar macrophages persist after the resolution of lung injury and fibrosis.** (A) Schematic of the experimental approach. Shielded bone marrow chimeras were harvested 10 mo after challenge with either bleomycin or with influenza A virus. (B) Percentage of cells identified as TR-AMs (CD45.2) and Mo-AMs (CD45.1) in untreated shielded chimeric mice, mice that received bleomycin, or mice infected with 100 PFU influenza A virus (A/WSN/33) as young adults (n = 3–5 mice per group; data are expressed as mean ± SEM). (C and D) 10 mo after the initial challenge, Mo-AMs and TR-AMs are no longer distinguishable by flow cytometry, and transcriptional profiling revealed only 330 differentially expressed genes (DEG; FDR step-up procedure q-value < 0.05; see Table S5). (E) Schematic illustration of the differential role of TR-AMs and Mo-AMs during the different stages of the lung injury and fibrosis.

TR-AMs than in TR-AMs isolated during fibrosis (*Pparg*, *Tgm2*, *Cebpb*, and *Tgfb1*). Collectively, these results show that Mo-AMs and TR-AMs alter their expression of both M1 and M2 genes during bleomycin-induced fibrosis and argue against an exclusive role for macrophage polarization toward a M2 phenotype to explain their contribution.

It is not known whether the alveolar macrophage pool is restored after the resolution of injury through the persistence of Mo-AMs recruited to the lung or whether TR-AMs proliferate to repopulate the alveolar macrophage pool. Bleomycin-induced fibrosis in young mice slowly resolves over 60 d (Hecker et al., 2014). Accordingly, we treated shielded bone marrow chimeric mice with bleomycin and measured the ratio between Mo-AMs and TR-AMs 10 mo later. Extending the findings from several groups (Guilliams et al., 2013; Hashimoto et al., 2013; van de Laar et al., 2016), we found that TR-AMs were remarkably stable, constituting >95% of alveolar macrophages at 14 mo of age (Fig. 7, A and B). In contrast, in mice that received bleomycin at 8 wk post–bone marrow transfer (4 mo of age), 10 mo later, ∼50% of the alveolar macrophages were monocyte derived. To determine whether this finding was unique to bleomycin, we treated a separate cohort of shielded bone marrow chimeric mice with influenza A (A/WSN/33) virus, at a dose that was associated with severe injury but was not lethal, and obtained similar results (Fig. 7 B). This finding suggests that a severe injury early in life can permanently reshape the alveolar macrophage landscape with respect to its developmental origins.

Next, we sought to determine whether the differences in gene expression between TR-AMs and Mo-AMs during fibrosis persisted over the life span. 10 mo after bleomycin treatment or influenza A infection, TR-AMs and Mo-AMs expressed similar levels of Siglec F and were no longer distinguishable by flow cytometry (Fig. 7 C). A comparison of the transcriptomes of TR-AMs and Mo-AMs 10 mo after bleomycin administration revealed only 330 differentially expressed genes (Fig. 7 D and Table S5).

The role of immune cell infiltration in the development of human lung fibrosis remains controversial. Therefore, we used flow cytometry to assess the number of alveolar macrophages in distal lung tissue obtained from the explanted lung, and a biopsy of the donor lung, in patients with lung fibrosis undergoing lung transplantation. We observed an expansion of alveolar macrophages in lung tissue samples from patients with fibrosis compared with the donor controls (Fig. 8, A and B; Bharat et al., 2016; Desch et al., 2016; Yu et al., 2016). Expansion of the alveolar macrophage pool was confirmed by immunostaining lung sections with the alveolar macrophage markers CD206 and CD169 (Fig. 8 C). As we found that Mo-AMs are causally linked to the development of lung fibrosis in response to bleomycin and Ad-TGF-β, we sought to determine whether the human homologues of the mouse profibrotic genes we identified in Mo-AMs during bleomycin-induced fibrosis (Fig. 5 C, cluster III) were up-regulated in alveolar macrophages isolated from the lungs of patients with lung fibrosis. We flow-sorted alveolar macrophages from

patients with end-stage lung fibrosis attributed to one of several etiologies (idiopathic pulmonary fibrosis, scleroderma-associated interstitial lung disease, polymyositis-associated interstitial lung disease, and mixed connective tissue disease) and alveolar macrophages from a small biopsy specimen of normal lung obtained from the donor, and we analyzed their transcriptome using RNA-seq. Of the genes differentially expressed in cluster III (Table S2), homologues of 61 genes were also differentially expressed between alveolar macrophages isolated from patients with lung fibrosis compared with donors: 51 were up-regulated in patients with lung fibrosis, including *APOE*, *ITGA6*, *FGFR1*, *MMP12*, *MMP14*, *PDPN*, and *SPARC* (Fig. 8 D; normalized counts in Table S6), which suggests the existence of common profibrotic pathways in human and mouse macrophages as well as highly conserved profibrotic alveolar macrophage signature across heterogeneous clinical entities. Several genes that were up-regulated in mouse Mo-AMs were down-regulated in patients with lung fibrosis, and some of these genes have been implicated in lung repair after injury (e.g., *CD163*, *MFGE8*, *LYVE1*, and *C1QB*). A pathogenic role for alveolar macrophages and other inflammatory cells has been dismissed because a human clinical trial showed the administration of corticosteroids was shown to have no effect or slightly worsened clinical outcomes in patients with idiopathic pulmonary fibrosis (Raghu et al., 2012). To determine whether corticosteroids targeted alveolar macrophages during the development of fibrosis, mice were treated with dexamethasone (equivalent prednisone dose of 1 mg/kg/day, intraperitoneal) beginning simultaneous with the administration of bleomycin. The severity of bleomycin-induced lung fibrosis in dexamethasone- and sham-treated mice was similar (Fig. S5, A–C). Dexamethasone treatment did not significantly alter the depletion of TR-AMs or the recruitment of Mo-AM during fibrosis (Fig. S5, D and E), consistent with the suggestion that corticosteroid treatment has little or no effect on the population of macrophages.

DISCUSSION

We used a genetic lineage tracing system to show that Mo-AMs and TR-AMs play distinct roles during the development of lung fibrosis. In common mouse models of lung fibrosis, the deletion of Mo-AM after their recruitment to the lung markedly attenuated the severity of fibrosis, whereas the deletion of TR-AM had no effect on fibrosis severity. These findings are bolstered by transcriptomic profiles of monocyte and macrophage populations over the course of bleomycin-induced fibrosis, which reveal substantial differences in gene expression between Mo-AMs and TR-AMs over the course of lung fibrosis. Our findings suggest revision of our consideration of alveolar macrophages as a single population of cells in the design of macrophage-targeted therapies in lung fibrosis.

Our transcriptomic data of flow-sorted monocyte and macrophage populations from lung homogenates suggest that monocyte to alveolar macrophage differentiation represents a continuous down-regulation of genes typically expressed in monocytes and up-regulation of genes expressed in alveolar macrophages. These findings suggest that monocytes give rise to interstitial macrophages, which in turn give rise to Mo-AMs, and are consistent with published data suggesting that monocyte to macrophage differentiation results from epigenetic reprogramming driven by factors present in the local microenvironment (Landsman and Jung, 2007; Lavin et al., 2014). We observed that the protection against bleomycin-induced lung fibrosis in both $Cre^{CD11c}Casp8^{floxflox}$ and $Cre^{LysM}Casp8^{floxflox}$ mice relative to $Casp8^{floxflox}$ controls. This protection was associated with preserved numbers of interstitial macrophages but a marked reduction in Mo-AMs. Caspase-8 initiates apoptosis through caspase-3/7 activation and blocks necroptosis via suppression of RIPK1–RIPK3 signaling (Hutcheson and Perlman, 2008; Oberst et al., 2011). The genetic loss of RIPK3 restored the population of Mo-AMs, and sensitivity to bleomycin induced fibrosis in caspase-8–deficient mice, suggesting these cells undergo necroptosis as they differentiate from interstitial macrophages to Mo-AMs. These results are consistent with previous studies that have demonstrated the importance of monocytes in the development of bleomycin-induced fibrosis (Gibbons et al., 2011; Larson-Casey et al., 2016) but represent an important advance with therapeutic implications. Systemic depletion of monocytes or inhibition of pathways required for monocyte migration to sites of tissue injury is necessarily limited by toxicity, as monocyte migration is required to maintain some tissue resident macrophage populations (e.g., in the gut) and for the systemic maintenance of dendritic cells (Lavin et al., 2015). Our data suggest that targeting pathways required for alveolar macrophage differentiation after monocytes have begun the process of differentiation in the lung can prevent fibrosis. Because many of these pathways are exclusively important for alveolar macrophages (Nakamura et al., 2013; Lavin et al., 2014; Schneider et al., 2014; Sennello et al., 2017), targeting them is predicted to slow the development of Mo-AMs without affecting monocyte or macrophage populations in other tissues.

Although TR-AMs increased the expression of some profibrotic genes during fibrosis, this response was substantially muted relative to Mo-AMs. We found that depletion of TR-AMs using intratracheal liposomal clodronate before the administration of bleomycin had no effect on fibrosis, suggesting they are dispensable for the development of fibrosis in this model. Furthermore, the significant protection we observed in $Cre^{CD11c}Casp8^{floxflox}$ and $Cre^{LysM}Casp8^{floxflox}$ mice cannot be attributed to deletion of caspase-8 in TR-AMs, as we found the TR-AMs in these mice had preserved expression of *Casp8*, suggesting they escaped genetic recombination. Indeed, there were few detectable differences in the transcriptomes of TR-AMs from $Cre^{CD11c}Casp8^{floxflox}$ and $Cre^{LysM}Casp8^{floxflox}$ mice compared with $Casp8^{floxflox}$ controls. Competitive chimera experiments and bone marrow reconstitution with $Cre^{CD11c}Casp8^{floxflox}RIPK3^{-/-}$ animals suggest

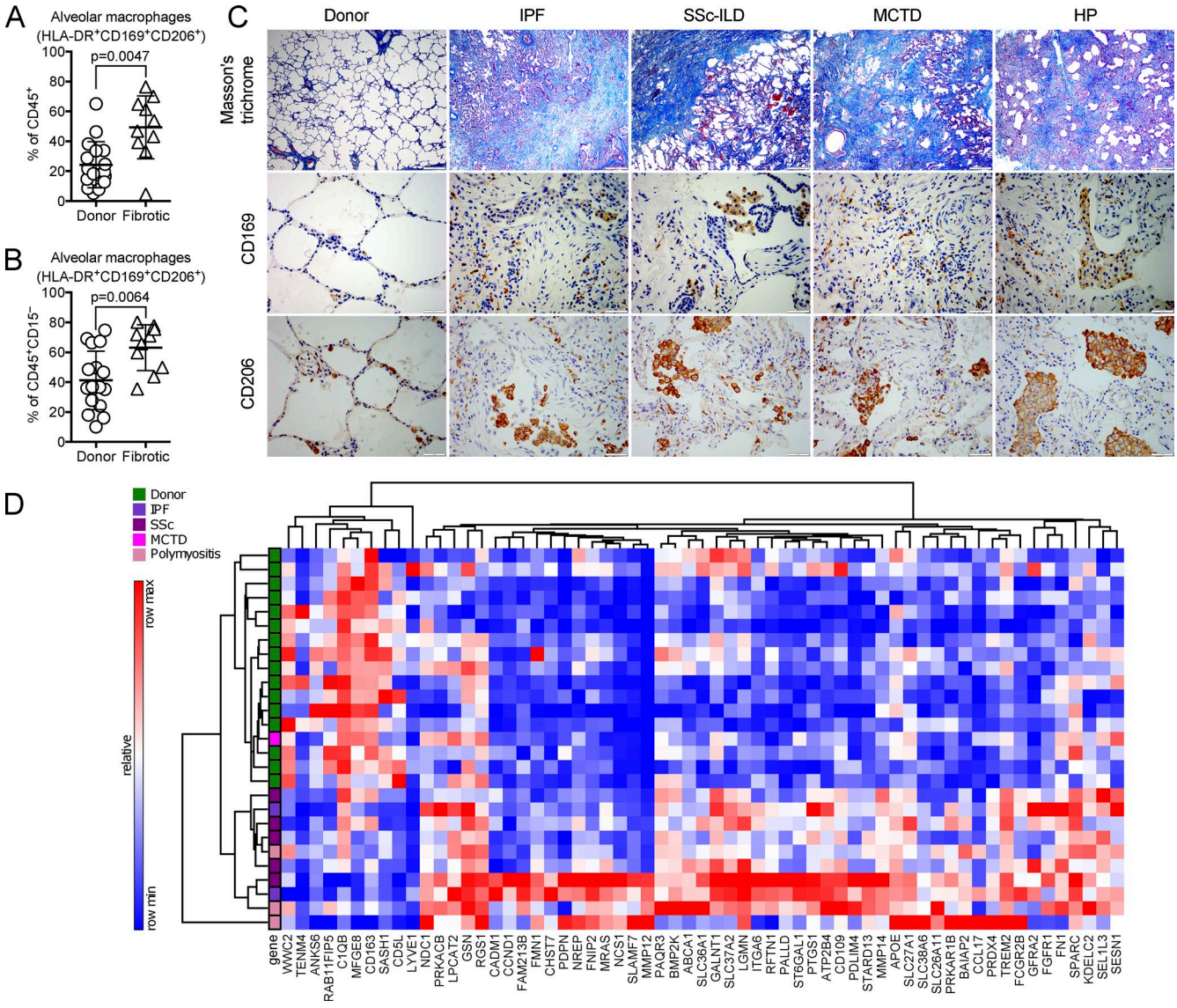

Figure 8. **Alveolar macrophages are expanded in patients with lung fibrosis and exhibit a profibrotic gene expression signature similar to mouse Mo-AMs during lung fibrosis.** (A–C) The population of alveolar macrophages is increased in patients with fibrotic lung disease. At the time of lung transplantation, small distal lung biopsy specimens were harvested from the donor lung (n = 16) and the recipient lung (n = 10) and processed for flow cytometry and immunohistochemistry. (A) Alveolar macrophages were identified as $CD206^+CD169^+HLA\text{-}DR^+$ cells out of all hematopoietic $CD45^+$ cells from donor lung tissue and from patients with lung fibrosis (Mann–Whitney test; data are expressed as mean ± SD). (B) The same analysis was repeated after excluding neutrophils (Mann–Whitney test; data are expressed as mean ± SD). (C, top) Masson's trichrome staining; bar, 500 µm. (C, middle) Immunohistochemistry for CD169; bar, 50 µm. (C, bottom) Immunohistochemistry for CD206; bar, 50 µm. Representative images from healthy donor, patients with idiopathic pulmonary fibrosis (IPF), systemic sclerosis-associated interstitial lung disease (SSc-ILD), mixed connective tissue disease (MCTD), and hypersensitivity pneumonitis (HP) are shown. (D) Of the differentially expressed genes in cluster III (Table S2), homologues of 61 were differentially expressed (FDR step-up procedure q-value < 0.05) between alveolar macrophages isolated from human fibrotic lung explants compared with donor lungs; 51 were up-regulated in patients with lung fibrosis, and 10 were down-regulated.

that in the absence of caspase-8, monocyte-derived cells (likely interstitial macrophages) undergo necroptosis as they differentiate into Mo-AMs. Although this suggests that RIPK is activated during alveolar macrophage differentiation, we were unable to identify a role for this pathway in fibrosis, as the transcriptomes of $Cre^{CD11c}Casp8^{floxflox}RIPK3^{-/-}$ Mo-AMs were similar to controls. Interestingly, although interstitial macrophages demonstrated even higher levels of profibrotic gene expression than Mo-AMs and their numbers were similar in $Cre^{CD11c}Casp8^{floxflox}$ and $Cre^{LysM}Casp8^{floxflox}$ mice compared with $Casp8^{floxflox}$ controls, protection against fibrosis was observed in the *Casp8*-deficient mice. This might reflect the

relatively low abundance of interstitial macrophages in comparison to Mo-AMs, a presumed difference in their life span, or their anatomical localization in the interstitium versus alveolar space, respectively.

It has long been known that complete depletion of alveolar macrophages with ionizing radiation results in their replacement by Mo-AMs that closely resemble TR-AMs (Hashimoto et al., 2013; Lavin et al., 2014; van de Laar et al., 2016). Although others have previously shown that monocytes recruited during the tissue injury can give rise to long-living self-renewing tissue-resident-like cells in the skin (Merad et al., 2002), it is not known whether Mo-AMs recruited to the lung during injury persist in the lung or whether the alveolar macrophage population is restored via proliferation of TR-AMs. We found that in the absence of injury, TR-AMs were a remarkably stable population, with <5% of cells originating from the bone marrow in 14-mo-old mice. In contrast, 1 yr after the administration of bleomycin, when fibrosis has completely resolved, ∼50% of alveolar macrophages were monocyte derived. Although Mo-AMs and TR-AMs showed marked differences in the expression of profibrotic genes during the development of fibrosis, 1 yr after fibrosis, they were indistinguishable by flow cytometry and showed only small differences in their transcriptome. Our design does not allow us to determine whether these retained Mo-AMs harbor an epigenetic memory of the inflammatory and fibrotic environment in which they were generated that is distinct from TR-AMs and respond differently to subsequent environmental challenges (Ostuni et al., 2013). Nevertheless, these results show that environmental exposures early in life can induce heterogeneity in the ontologic origins of alveolar macrophages, offering a possible mechanism to explain the enhanced and persistent fibrosis reported with repeated doses of bleomycin and during aging (Degryse et al., 2010; Hecker et al., 2014).

In lung transplant recipients examined up to 5 yr after transplantation, investigators reported that the majority of alveolar macrophages originated from the donor, suggesting the presence of a stable population of TR-AMs in humans analogous to those found in mice (Nayak et al., 2016). The decline in lung function in patients with fibrosis is not continuous, and step declines are often preceded by the development of "exacerbations," or an acute or subacute clinical worsening of shortness of breath and hypoxemia accompanied by inflammatory infiltrates on computed tomography imaging of the chest that suggest a role for immune cells in the pathogenesis of pulmonary fibrosis (Collard et al., 2007). However, a multicenter clinical trial of corticosteroids for the treatment of pulmonary fibrosis failed to show benefit, with a nonsignificant trend toward harm (Raghu et al., 2012). As a result of this trial and studies reporting that lung inflammation is sometimes worse in mice with genetic mutations that prevent the development of fibrosis, many concluded that inflammation is dispensable for the development of fibrosis (Munger et al., 1999; Budinger et al., 2006; Rock et al., 2011). Our data challenge these findings. We detected a substantial expansion in macrophages using newly described flow cytometry markers in distal lung tissue from a small number of patients with pulmonary fibrosis compared with normal lungs from the donor. Transcriptional profiling of these cells revealed substantial overlap in the expression of human homologues of the profibrotic genes up-regulated in Mo-AMs in mice exposed to bleomycin. This led us to examine the effect of corticosteroids on macrophages in lung fibrosis. Similar to the human trial, corticosteroids had no effect on the severity of bleomycin-induced lung fibrosis; however, we found that neither the TR-AM nor the Mo-AM population was affected by steroid treatment.

Our study has several limitations. Although the approach we used is a powerful tool to identify the sequence of transcriptional modifications that develop during monocyte to macrophage differentiation during disease, pulsed lineage tracing techniques will be required to follow an individual population of monocytes during their differentiation into Mo-AMs (Paul et al., 2015). Second, our flow cytometry approach cannot provide anatomical detail, except when antibodies for immunofluorescence or immunohistochemistry are available. For example, it is possible that Mo-AMs that persist in the lung after injury are differentially localized to areas where the microenvironment is subtly abnormal. Third, although our data suggest that the concept of M2 polarization overly simplifies the complex changes in gene expression that occur in both Mo-AMs and TR-AMs over the course of lung fibrosis (Nahrendorf and Swirski, 2016), it is possible that a subpopulation of Mo-AMs with one of these signatures or at different developmental stages contributed disproportionately to the fibrotic gene expression signature. Single-cell RNA-seq analysis will be required to exclude this possibility. Fourthly, the Cre^{LysM} and Cre^{CD11c} promoters both target dendritic cells. Therefore, although we did not see changes in the numbers of dendritic cells in the lungs of the caspase-8–deficient mice generated using these promoters, we cannot exclude the possibility that some of the effects we observed are attributable to dendritic cells. Finally, although we are unaware of previous studies showing an expansion of the alveolar macrophage pool in patients with lung fibrosis or previous studies of transcriptional profiling of these cells during fibrosis, we cannot determine whether they play a causal role in disease pathogenesis.

In summary, our results suggest that an appreciation of macrophage heterogeneity has important implications for disease pathogenesis and therapeutic development. Mo-AMs undergo dramatic transcriptional changes as they differentiate in the injured lung through a process that unfolds slowly over time. Mo-AMs express consistently higher levels of proinflammatory and profibrotic genes than TR-AMs, and selective depletion of Mo-AMs, but not TR-AMs, ameliorates the severity of lung fibrosis. Profibrotic gene expression in Mo-AMs harvested from mice during fibrosis is homologous to genes differentially regulated in alveolar macrophages from patients

with lung fibrosis. These results challenge the consideration alveolar macrophages during lung fibrosis as a single population of M2 polarized macrophages and suggest that selectively targeting Mo-AMs after their commitment to an alveolar macrophage fate may ameliorate fibrosis without the off-target effects of therapies that deplete circulating monocytes. Our finding that Mo-AMs persist in the lung after the resolution of injury shows that environmental exposures can permanently change the origins of alveolar macrophages. Determining whether retained Mo-AMs and TR-AMs respond differently to a subsequent injury or differentially change their gene expression signature with age may offer a mechanism to understand the increased risk of lung fibrosis with advancing age.

MATERIALS AND METHODS

Human subjects

All human studies were approved by Northwestern IRB and Department of Defense Human Research Protection Office. All human subjects provided written informed consent before enrolment into the study. A biopsy-size piece of the donor lung tissue and a lobe of the explanted recipient lung were obtained at the time of the lung transplant. Tissues were processed for flow cytometry and histology as previously described (Bharat et al., 2016). 10 patients with fibrotic lung disease (2 patients with idiopathic pulmonary fibrosis, 5 patients with systemic sclerosis-associated interstitial lung disease, 1 patient with mixed connective tissue disease, 1 patient with interstitial pneumonitis, and 1 patient with pneumoconiosis) were included in flow cytometric analysis.

Mice

All mouse procedures were approved by the Institutional Animal Care and Use Committee at Northwestern University. The mouse strains C57BL/6, B6.SJL-*Ptprc*^{a} *Pepc*^{b}/BoyJ (CD45.1) were used. All strains including wild-type mice are bred and housed at a barrier- and specific pathogen–free facility at the Center for Comparative Medicine at Northwestern University (Chicago, IL). Colonies are refreshed at least yearly with mice purchased from The Jackson Laboratory. 8–10-wk-old mice were used for all experiments, although some were aged up to 14 mo in our facility. *Casp8*$^{flox/flox}$, *CD11c*^{Cre}*Casp8*$^{flox/flox}$, *LysM*^{Cre}*Casp8*$^{flox/flox}$, *CD11c*^{Cre}*Casp8*$^{flox/flox}$*RIPK3*$^{-/-}$, and *LysM*^{Cre}*Casp8*$^{flox/flox}$*RIPK3*$^{-/-}$ mice were described previously (Cuda et al., 2014, 2015); these mice were backcrossed to C57BL/6 background for >10 generations. Littermate controls were used in all experiments, except for generation of competitive bone marrow chimeras. All procedures were approved by the Institutional Animal Care and Use committee at Northwestern University. Bleomycin-induced lung fibrosis, TGF-β–induced lung fibrosis, and influenza A virus infection (A/WSN/33) were performed and assessed as previously described (Budinger et al., 2006; Misharin et al., 2013; Morales-Nebreda et al., 2014, 2015; Sennello et al., 2017).

Tissue preparation and flow cytometry

Tissue preparation for flow cytometry analysis and cell sorting was performed as previously described (Misharin et al., 2013, 2014; Bharat et al., 2016). Blood was collected into EDTA-containing tubes via facial vein bleed (from live animals) or cardiac puncture (from euthanized animals). Whole blood was stained with fluorochrome-conjugated antibodies, and erythrocytes were then lysed using BD FACS lysing solution. For single-cell suspension obtained from tissues erythrocytes were lysed using BD Pharm Lyse, and cells were counted using Countess automated cell counter (Invitrogen); dead cells were discriminated using trypan blue. Cells were stained with eFluor 506 (eBioscience) viability dyes, incubated with FcBlock (BD), and stained with fluorochrome-conjugated antibodies (antibodies, clones, fluorochromes, and manufacturers were described in detail in our previous publications; Misharin et al., 2013, 2014; Bharat et al., 2016). Data were acquired on BD LSR II flow cytometer (for information regarding instrument configuration and antibody panels, see Misharin et al., 2013, 2014; Bharat et al., 2016). Compensation, analysis and visualization of the flow cytometry data were performed using FlowJo software (Tree Star). "Fluorescence minus one" controls were used when necessary to set up gates. Cell sorting was performed at Northwestern University RLHCCC Flow Cytometry core facility on SORP FAC SAria III instrument (BD) with the same optical configuration as LSR II, using a 100-µm nozzle and 40 psi pressure.

Bone marrow chimeras and shielded bone marrow chimeras

Bone marrow chimeras were established by transferring 5×10^6 bone marrow cells isolated from C57BL/6 mice (this strain expresses CD45.2 alloantigen) into 8-wk-old lethally irradiated (single dose of 1,000 cGy γ-radiation using a Cs-137–based Gammacell-40 irradiator; Nordion) recipient mice (expressing CD45.1 alloantigen). Mice were maintained on autoclaved water supplemented with antibiotics (trimethoprim/sulfamethoxazole; Hi-Tech Pharmacal) for 4 wk after bone marrow transfer and then switched to normal housing regimen. CD45.2 to CD45.1 bone marrow chimeras were used for experiments 8 wk after bone marrow transfer. 8 wk after bone marrow transfer, >95% of all leukocytes and 100% of monocytes and neutrophils in peripheral blood were of donor origin. Bone marrow chimeras with thoracic shielding were used to assess the origin of pulmonary macrophages (TR-AMs vs. Mo-AMs) and were generated in a manner similar to that previously described (Janssen et al., 2011), with additional modifications (Misharin et al., 2014). To protect TR-AMs from radiation, we applied a uniform lead shield that covered the lungs during irradiation as previously described using a custom-made "Mousotron-5" apparatus. However, we found this approach was limited, as the residual recipient bone marrow in the shielded region results in incomplete chimerism; ∼20% of peripheral blood monocytes are still of recipient origin and cannot be distinguished from tissue-resident macrophages upon recruitment to the lung. This problem was corrected by the administration the myeloablative agent busulfan (30 mg/kg

body weight; Sigma-Aldrich; Chevaleyre et al., 2013) 6 h after the irradiation, followed 12 h later by bone marrow infusion. 2 mo after the procedure, 100% of all alveolar macrophages in the shielded bone marrow chimeras were of recipient origin (CD45.2), whereas 100% of all circulating monocytes were of donor origin (CD45.1). Bone marrow chimeras with thoracic shielding were maintained on antibiotics for 4 wk as described above and then switched back to the normal housing regimen.

Gene expression profiling (RNA-seq) and bioinformatic analysis

In the overall design, monocyte and macrophage subpopulations were isolated from naive, bleomycin-, or influenza A virus–challenged mice at the indicated time points via FACS-sorting on BD FACSAria III instrument and RNA was extracted for subsequent transcriptomic analysis. For each genotype/condition, two to five biological replicates were used. Libraries for RNA-seq were prepared in 96-well plate format. For the bleomycin time-course experiment, 155 samples were equally distributed between two batches of the libraries preparation (78 and 77 samples), so each group/condition would be represented on each plate. For experiments using shielded chimeras with busulfan (40 samples), libraries were prepared as a single batch.

Monocyte and macrophage subpopulations were isolated on BD FACSAria III instrument, 0.5–1.5 × 10^5 cells were sorted into capture media (PBS, 2% BSA and 0.05% EDTA), immediately spun down and lysed in 350 µl of RLT-plus buffer (QIAGEN) supplemented with β2-mercaptoethanol. Total RNA was extracted using RNeasy Plus Mini kit (QIAGEN) and eluted in 35 µl of nuclease free water. RNA quality and quantity were assessed using Bioanalyzer 2100 or TapeStation 4200 instruments (Agilent Technologies). RNA-seq libraries were prepared in 96-well plate format using NEBNext Poly(A) mRNA Magnetic Isolation Module, NEBNext Ultra RNA Library Prep kit for Illumina and NEBNext Multiplex Oligos for Illumina (Dual Index Primers Set 1) according to the standard protocol. 50 ng total RNA was enriched for poly(A) mRNA using NEBNext Poly(A) mRNA Magnetic Isolation Module, the mRNA was subjected to chemical fragmentation in the presence of divalent cations at 94°C for 15 min, and cDNA was generated using random primers and ProtoScript II reverse transcription in the presence of mouse RNase inhibitor using the following program: 10 min at 25°C, 15 min at 42°C, and 15 min and 70°C. Second-strand DNA was generated using NEBNext Second Strand Synthesis Enzyme module (DNA polymerase I, RNase H, *Escherichia coli* DNA ligase) for 60 min at 16°C. The resulting double-stranded DNA was purified using 1.8× volume of SPRI beads (AMPure XP Beads; Beckman Coulter) or HighPrep PCR Beads (MagBio Genomics), eluted in 0.1× TE (Tris/EDTA) buffer, DNA ends were repaired using NEBNext End Prep Enzyme Mix (T4 PNK and T4 DNA polymerase) for 30 min at 20°C and 30 min and 65°C, followed by NEBNext adaptor for Illumina ligation using Blunt/TA Ligase master mix (T4 DNA ligase) for 15 min at 20°C and incubation with USER enzyme for 15 min at 37°C. After another round of purification using 1× volume of SPRI Beads, adaptor-ligated DNA was amplified using NEBNext Q5 Hot Start HiFi DNA polymerase in the presence of NEBNext multiplex oligos (dual index primers) for 14 cycles. PCR-enriched libraries were purified using a 0.9× volume of SPRI Beads, and their quality was assessed using Bioanalyzer 2100 or TapeStation 4200 instruments. Equimolar amount of libraries were pooled and sequenced on Illumina NextSeq 500 instrument (single end reads) using V1 chemistry high-output 150 cycles sequencing kit (bleomycin time-course experiment) or V2 chemistry 75 cycles high-output sequencing kit (aged-shielded bone marrow chimeras).

Computation intensive analysis was performed using "Genomics Nodes" on Northwestern's High Performance Computing Cluster, Quest (Northwestern IT and Research Computing). Reads were demultiplexed using bcl2fastc, quality was assessed using FastQC, reads were trimmed and aligned to mm10 reference genome using TopHat2, read counts were associated with genes using the GenomicRanges (Lawrence et al., 2013), and differential gene expression was assessed using edgeR (Robinson et al., 2010; McCarthy et al., 2012) R/Bioconductor packages. Genes with less than one normalized read count across at least half of the samples were filtered from all analyses. Pearson correlation matrix and clustering heat maps were built using GENE-E (J. Gould, 2013; GENE.E: Interact with GENE-E from R. R package version 1.12.2; http://www.broadinstitute.org/cancer/software/GENE-E). Gene ontologies were evaluated using GOrilla (Eden et al., 2007, 2009). The dataset is available on the GEO database under accession number GSE82158.

Statistical analysis

For all fibrosis measurements, the data were analyzed using two-way ANOVA for repeated measurements with Bonferroni post-test to compare differences between the groups. All analyses were performed using GraphPad Prism version 7.00 (GraphPad Software). Data are shown as means ± SEM.

Online supplemental material

Fig. S1 shows the gating strategy used to isolate subsets of monocytes and macrophages during the course of bleomycin-induced lung fibrosis. Fig. S2 shows data demonstrating protection from Ad-TGFb-induced lung fibrosis in *Casp8*-deficient mice. Fig. S3 shows global transcriptome differences between populations of macrophages and relevant GO processes. Fig. S4 (related to Fig. 6) shows differences between TR-AMs and Mo-AMs at day 19 of bleomycin-induced lung fibrosis and absence of evidence supporting clear M1/M2 pattern of macrophage polarization in vivo. Fig. S5 shows glucocorticoids have no effect on the course of bleomycin-induced lung fibrosis. Table S1 (related to Fig. 5 and Fig. S3) contains Pearson's correlation coefficients for transcriptomes of the individual macrophage populations. Table S2 (related to Fig. 5) contains

k-means cluster assignment. Table S3 (related to Fig. 5 and Fig. S3) contains GO processes and statistics for each cluster. Table S4 (related to Fig. 6) contains results of Fgnet enrichment. Table S5 (related to Fig. 7) contains list of differentially expressed genes between TR-AMs and Mo-AMs 10 mo after bleomycin-induced lung fibrosis. Table S6 (related to Fig. 8) contains normalized gene counts for human homologues of the mouse genes from cluster III. Tables S1–S6 are included as Excel files.

ACKNOWLEDGMENTS

A.V. Misharin is supported by National Institutes of Health (NIH) National Institute of Arthritis and Musculoskeletal and Skin Diseases grant AR061593, an American Thoracic Society/Scleroderma Foundation research grant, Department of Defense grant PR141319, and a BD Bioscience immunology research grant. P.A. Reyfman is supported by Northwestern University's Lung Sciences Training Program (5T32 HL076139-13). C.M. Cuda is supported by NIH grant AR064313. S. Chiu is supported by Northwestern University's Transplant Surgery Scientist Training Program (NIH grant T32 DK077662) and the American Society for Transplant Surgery Foundation. A. Bharat is supported by NIH grant HL125940 and matching funds from Thoracic Surgery Foundation, a research grant from the Society of University Surgeons, and an American Association of Thoracic Surgery John H. Gibbon Jr. Research Scholarship. B.D. Singer is supported by NIH grant HL128867 and the Parker B. Francis Research Opportunity Award. J.I. Sznajder is supported by NIH grants AG049665, HL048129, HL071643, and HL085534. G. Multlu is supported by NIH grants ES015024 and ES025644. K. Ridge is supported by NIH grants HL079190 and HL124664. G.R.S. Budinger is supported by NIH grants ES013995, HL071643, and AG049665; Veterans Administration grant BX000201, and Department of Defense grant PR141319. H. Perlman is supported by NIH grants AR064546, AG049665, and HL134375 and funds provided by Mabel Greene Myers Chair. The Northwestern University Flow Cytometry Facility and Center for Advanced Microscopy are supported by a National Cancer Institute cancer center support grant P30 CA060553 awarded to the Robert H. Lurie Comprehensive Cancer Center. The Genomics Computing Cluster is jointly supported by the Feinberg School of Medicine, the Center for Genetic Medicine, and Feinberg's Department of Biochemistry and Molecular Genetics, the Office of the Provost, the Office for Research, and Northwestern Information Technology and maintained and developed by Feinberg IT and Research Computing Group.

The authors declare no competing financial interests.

Author contributions: A.V. Misharin contributed to conceptualization, methodology, validation, formal analysis, investigation, resources, data curation, writing, visualization, supervision, project administration, and funding acquisition. L. Morales-Nebreda contributed to conceptualization, methodology, validation, formal analysis, investigation, data curation, writing, and visualization. P.A. Reyfman contributed to conceptualization, methodology, software, validation, formal analysis, investigation, data curation, writing, visualization, and supervision. T.J. Yacoub contributed to conceptualization, methodology, software, validation, formal analysis, data curation, writing, and visualization. C.M. Cuda contributed to conceptualization, methodology, validation, formal analysis, investigation, resources, data curation, and writing. H. Abdala-Valencia contributed to investigation, resources, data analysis, data curation, writing, visualization, and project administration. J.M. Walter contributed to formal analysis, investigation, data curation, writing, and visualization. A.C. McQuattie-Pimentel contributed to methodology, validation, formal analysis, investigation, data curation, and writing. C. Chen contributed to methodology, validation, formal analysis, investigation, and data curation. N. Joshi contributed to methodology, validation, formal analysis, investigation, and data curation. K.J.N. Williams contributed to methodology, validation, formal analysis, investigation, and data curation. M. Chi contributed to methodology, validation, formal analysis, investigation, and data curation. S. Chiu contributed to methodology, validation, formal analysis, investigation, data curation, and writing. F.J. Gonzalez-Gonzalez contributed to methodology, validation, formal analysis, investigation, and data curation. K. Gates contributed to methodology, validation, formal analysis, investigation, and data curation. A.P. Lam contributed to methodology, validation, formal analysis, investigation, and data curation. T.T. Nicholson contributed to investigation and data curation. P.J. Homan contributed to methodology, validation, formal analysis, investigation, and data curation. S. Soberanes contributed to methodology, validation, formal analysis, investigation, and data curation. S. Dominguez contributed to methodology, validation, and investigation. V.K. Morgan contributed to methodology, validation, investigation, and data curation. R. Saber contributed to validation, formal analysis, investigation, and data curation. A. Shaffer contributed to validation, formal analysis, investigation, and data curation. K.R. Anekalla contributed to methodology, software, validation, formal analysis, investigation, data curation, writing, and visualization. S.A. Marshall contributed to methodology, formal analysis, and investigation. M. Hinchcliff contributed to resources, data curation, writing, and supervision. A. Bharat contributed to resources, data curation, writing, and supervision. S.M. Bhorade contributed to resources, data curation, writing, and supervision. B.D. Singer and S. Berdnikovs contributed to methodology, validation, formal analysis, writing, and visualization. E.T. Bartom contributed to methodology, validation, software, and formal analysis. W.E. Balch contributed to conceptualization, resources, data curation, writing, supervision, and project administration. R.I. Morimoto contributed to conceptualization, resources, data curation, writing, and supervision, project administration. J.I. Sznajder contributed to conceptualization, resources, data curation, writing, supervision, and project administration. N.S. Chandel contributed to conceptualization, data curation, writing, and supervision. G.M. Mutlu contributed to conceptualization, resources, data curation, writing, and supervision. M. Jain contributed to conceptualization, data curation, writing, and supervision. C.J. Gottardi contributed to conceptualization, resources, writing, supervision, and project administration. K.M. Ridge contributed to conceptualization, resources, writing, supervision, and project administration. N. Bagheri contributed to conceptualization, methodology, formal analysis, resources, data curation, writing, and visualization. A. Shilatifard contributed to methodology, resources. GR.S. Budinger contributed to conceptualization, methodology, validation, formal analysis, investigation, resources, data curation, writing, visualization, supervision, project administration, and funding acquisition. H. Perlman contributed to conceptualization, methodology, validation, formal analysis, investigation, resources, data curation, writing, visualization, supervision, project administration, funding acquisition.

Submitted: 19 December 2016
Revised: 2 April 2017
Accepted: 25 May 2017

REFERENCES

Agassandian, M., J.R. Tedrow, J. Sembrat, D.J. Kass, Y. Zhang, E.A. Goncharova, N. Kaminski, R.K. Mallampalli, and L.J. Vuga. 2015. VCAM-1 is a TGF-β1 inducible gene upregulated in idiopathic pulmonary fibrosis. *Cell. Signal.* 27:2467–2473. http://dx.doi.org/10.1016/j.cellsig.2015.09.003

Aibar, S., C. Fontanillo, C. Droste, and J. De Las Rivas. 2015. Functional Gene Networks: R/Bioc package to generate and analyse gene networks derived from functional enrichment and clustering. *Bioinformatics.* 31:1686–1688. http://dx.doi.org/10.1093/bioinformatics/btu864

Aschner, Y., A.P. Khalifah, N. Briones, C. Yamashita, L. Dolgonos, S.K. Young, M.N. Campbell, D.W. Riches, E.F. Redente, W.J. Janssen, et al. 2014. Protein tyrosine phosphatase α mediates profibrotic signaling in lung fibroblasts through TGF-β responsiveness. *Am. J. Pathol.* 184:1489–1502. http://dx.doi.org/10.1016/j.ajpath.2014.01.016

Bharat, A., S.M. Bhorade, L. Morales-Nebreda, A.C. McQuattie-Pimentel, S. Soberanes, K. Ridge, M.M. DeCamp, K.K. Mestan, H. Perlman, G.R. Budinger, and A.V. Misharin. 2016. Flow cytometry reveals similarities between lung macrophages in humans and mice. *Am. J. Respir. Cell Mol. Biol.* 54:147–149. http://dx.doi.org/10.1165/rcmb.2015-0147LE

Brodeur, T.Y., T.E. Robidoux, J.S. Weinstein, J. Craft, S.L. Swain, and A. Marshak-Rothstein. 2015. IL-21 promotes pulmonary fibrosis through the induction of profibrotic CD8+ T cells. *J. Immunol.* 195:5251–5260. http://dx.doi.org/10.4049/jimmunol.1500777

Budinger, G.R., G.M. Mutlu, J. Eisenbart, A.C. Fuller, A.A. Bellmeyer, C.M. Baker, M. Wilson, K. Ridge, T.A. Barrett, V.Y. Lee, and N.S. Chandel. 2006. Proapoptotic Bid is required for pulmonary fibrosis. *Proc. Natl. Acad. Sci. USA.* 103:4604–4609. http://dx.doi.org/10.1073/pnas.0507604103

Chan, M.F., J. Li, A. Bertrand, A.J. Casbon, J.H. Lin, I. Maltseva, and Z. Werb. 2013. Protective effects of matrix metalloproteinase-12 following

corneal injury. *J. Cell Sci.* 126:3948–3960. http://dx.doi.org/10.1242/jcs.128033

Chevaleyre, J., P. Duchez, L. Rodriguez, M. Vlaski, A. Villacreces, V. Conrad-Lapostolle, V. Praloran, Z. Ivanovic, and P. Brunet de la Grange. 2013. Busulfan administration flexibility increases the applicability of scid repopulating cell assay in NSG mouse model. *PLoS One.* 8:e74361. http://dx.doi.org/10.1371/journal.pone.0074361

Collard, H.R., B.B. Moore, K.R. Flaherty, K.K. Brown, R.J. Kaner, T.E. King Jr., J.A. Lasky, J.E. Loyd, I. Noth, M.A. Olman, et al. Idiopathic Pulmonary Fibrosis Clinical Research Network Investigators. 2007. Acute exacerbations of idiopathic pulmonary fibrosis. *Am. J. Respir. Crit. Care Med.* 176:636–643. http://dx.doi.org/10.1164/rccm.200703-463PP

Cuda, C.M., A.V. Misharin, A.K. Gierut, R. Saber, G.K. Haines III, J. Hutcheson, S.M. Hedrick, C. Mohan, G.S. Budinger, C. Stehlik, and H. Perlman. 2014. Caspase-8 acts as a molecular rheostat to limit RIPK1- and MyD88-mediated dendritic cell activation. *J. Immunol.* 192:5548–5560. http://dx.doi.org/10.4049/jimmunol.1400122

Cuda, C.M., A.V. Misharin, S. Khare, R. Saber, F. Tsai, A.M. Archer, P.J. Homan, G.K. Haines III, J. Hutcheson, A. Dorfleutner, et al. 2015. Conditional deletion of caspase-8 in macrophages alters macrophage activation in a RIPK-dependent manner. *Arthritis Res. Ther.* 17:291. http://dx.doi.org/10.1186/s13075-015-0794-z

Dannappel, M., K. Vlantis, S. Kumari, A. Polykratis, C. Kim, L. Wachsmuth, C. Eftychi, J. Lin, T. Corona, N. Hermance, et al. 2014. RIPK1 maintains epithelial homeostasis by inhibiting apoptosis and necroptosis. *Nature.* 513:90–94. http://dx.doi.org/10.1038/nature13608

Degryse, A.L., H. Tanjore, X.C. Xu, V.V. Polosukhin, B.R. Jones, F.B. McMahon, L.A. Gleaves, T.S. Blackwell, and W.E. Lawson. 2010. Repetitive intratracheal bleomycin models several features of idiopathic pulmonary fibrosis. *Am. J. Physiol. Lung Cell. Mol. Physiol.* 299:L442–L452. http://dx.doi.org/10.1152/ajplung.00026.2010

Desch, A.N., S.L. Gibbings, R. Goyal, R. Kolde, J. Bednarek, T. Bruno, J.E. Slansky, J. Jacobelli, R. Mason, Y. Ito, et al. 2016. Flow cytometric analysis of mononuclear phagocytes in nondiseased human lung and lung-draining lymph nodes. *Am. J. Respir. Crit. Care Med.* 193:614–626. http://dx.doi.org/10.1164/rccm.201507-1376OC

Eden, E., D. Lipson, S. Yogev, and Z. Yakhini. 2007. Discovering motifs in ranked lists of DNA sequences. *PLOS Comput. Biol.* 3:e39. http://dx.doi.org/10.1371/journal.pcbi.0030039

Eden, E., R. Navon, I. Steinfeld, D. Lipson, and Z. Yakhini. 2009. GOrilla: A tool for discovery and visualization of enriched GO terms in ranked gene lists. *BMC Bioinformatics.* 10:48. http://dx.doi.org/10.1186/1471-2105-10-48

Fan, D., A. Takawale, R. Basu, V. Patel, J. Lee, V. Kandalam, X. Wang, G.Y. Oudit, and Z. Kassiri. 2014. Differential role of TIMP2 and TIMP3 in cardiac hypertrophy, fibrosis, and diastolic dysfunction. *Cardiovasc. Res.* 103:268–280. http://dx.doi.org/10.1093/cvr/cvu072

Fiorotto, R., A. Villani, A. Kourtidis, R. Scirpo, M. Amenduni, P.J. Geibel, M. Cadamuro, C. Spirli, P.Z. Anastasiadis, and M. Strazzabosco. 2016. The cystic fibrosis transmembrane conductance regulator controls biliary epithelial inflammation and permeability by regulating Src tyrosine kinase activity. *Hepatology.* 64:2118–2134. http://dx.doi.org/10.1002/hep.28817

Flechsig, P., B. Hartenstein, S. Teurich, M. Dadrich, K. Hauser, A. Abdollahi, H.J. Gröne, P. Angel, and P.E. Huber. 2010. Loss of matrix metalloproteinase-13 attenuates murine radiation-induced pulmonary fibrosis. *Int. J. Radiat. Oncol. Biol. Phys.* 77:582–590. http://dx.doi.org/10.1016/j.ijrobp.2009.12.043

Fontanillo, C., R. Nogales-Cadenas, A. Pascual-Montano, and J. De las Rivas. 2011. Functional analysis beyond enrichment: non-redundant reciprocal linkage of genes and biological terms. *PLoS One.* 6:e24289. http://dx.doi.org/10.1371/journal.pone.0024289

Gautier, E.L., T. Shay, J. Miller, M. Greter, C. Jakubzick, S. Ivanov, J. Helft, A. Chow, K.G. Elpek, S. Gordonov, et al. Immunological Genome Consortium. 2012. Gene-expression profiles and transcriptional regulatory pathways that underlie the identity and diversity of mouse tissue macrophages. *Nat. Immunol.* 13:1118–1128. http://dx.doi.org/10.1038/ni.2419

Gibbings, S.L., R. Goyal, A.N. Desch, S.M. Leach, M. Prabagar, S.M. Atif, D.L. Bratton, W. Janssen, and C.V. Jakubzick. 2015. Transcriptome analysis highlights the conserved difference between embryonic and postnatal-derived alveolar macrophages. *Blood.* 126:1357–1366. http://dx.doi.org/10.1182/blood-2015-01-624809

Gibbons, M.A., A.C. MacKinnon, P. Ramachandran, K. Dhaliwal, R. Duffin, A.T. Phythian-Adams, N. van Rooijen, C. Haslett, S.E. Howie, A.J. Simpson, et al. 2011. Ly6Chi monocytes direct alternatively activated profibrotic macrophage regulation of lung fibrosis. *Am. J. Respir. Crit. Care Med.* 184:569–581. http://dx.doi.org/10.1164/rccm.201010-1719OC

Grgic, I., E. Kiss, B.P. Kaistha, C. Busch, M. Kloss, J. Sautter, A. Müller, A. Kaistha, C. Schmidt, G. Raman, et al. 2009. Renal fibrosis is attenuated by targeted disruption of KCa3.1 potassium channels. *Proc. Natl. Acad. Sci. USA.* 106:14518–14523. http://dx.doi.org/10.1073/pnas.0903458106

Guilliams, M., I. De Kleer, S. Henri, S. Post, L. Vanhoutte, S. De Prijck, K. Deswarte, B. Malissen, H. Hammad, and B.N. Lambrecht. 2013. Alveolar macrophages develop from fetal monocytes that differentiate into long-lived cells in the first week of life via GM-CSF. *J. Exp. Med.* 210:1977–1992. http://dx.doi.org/10.1084/jem.20131199

Hashimoto, D., A. Chow, C. Noizat, P. Teo, M.B. Beasley, M. Leboeuf, C.D. Becker, P. See, J. Price, D. Lucas, et al. 2013. Tissue-resident macrophages self-maintain locally throughout adult life with minimal contribution from circulating monocytes. *Immunity.* 38:792–804. http://dx.doi.org/10.1016/j.immuni.2013.04.004

Hecker, L., N.J. Logsdon, D. Kurundkar, A. Kurundkar, K. Bernard, T. Hock, E. Meldrum, Y.Y. Sanders, and V.J. Thannickal. 2014. Reversal of persistent fibrosis in aging by targeting Nox4-Nrf2 redox imbalance. *Sci. Transl. Med.* 6:231ra47. http://dx.doi.org/10.1126/scitranslmed.3008182

Hutcheson, J., and H. Perlman. 2008. BH3-only proteins in rheumatoid arthritis: Potential targets for therapeutic intervention. *Oncogene.* 27:S168–S175. http://dx.doi.org/10.1038/onc.2009.54

Ishizuka, H., V. García-Palacios, G. Lu, M.A. Subler, H. Zhang, C.S. Boykin, S.J. Choi, L. Zhao, K. Patrene, D.L. Galson, et al. 2011. ADAM8 enhances osteoclast precursor fusion and osteoclast formation in vitro and in vivo. *J. Bone Miner. Res.* 26:169–181. http://dx.doi.org/10.1002/jbmr.199

Janssen, W.J., L. Barthel, A. Muldrow, R.E. Oberley-Deegan, M.T. Kearns, C. Jakubzick, and P.M. Henson. 2011. Fas determines differential fates of resident and recruited macrophages during resolution of acute lung injury. *Am. J. Respir. Crit. Care Med.* 184:547–560. http://dx.doi.org/10.1164/rccm.201011-1891OC

Kim, S.Y., B.H. Cho, and U.H. Kim. 2010. CD38-mediated Ca2+ signaling contributes to angiotensin II-induced activation of hepatic stellate cells: attenuation of hepatic fibrosis by CD38 ablation. *J. Biol. Chem.* 285:576–582. http://dx.doi.org/10.1074/jbc.M109.076216

Kopf, M., C. Schneider, and S.P. Nobs. 2015. The development and function of lung-resident macrophages and dendritic cells. *Nat. Immunol.* 16:36–44. http://dx.doi.org/10.1038/ni.3052

Lai, C.F., S.L. Lin, W.C. Chiang, Y.M. Chen, V.C. Wu, G.H. Young, W.J. Ko, M.L. Kuo, T.J. Tsai, and K.D. Wu. 2014. Blockade of cysteine-rich protein 61 attenuates renal inflammation and fibrosis after ischemic kidney injury. *Am. J. Physiol. Renal Physiol.* 307:F581–F592. http://dx.doi.org/10.1152/ajprenal.00670.2013

Lam, A.P., J.D. Herazo-Maya, J.A. Sennello, A.S. Flozak, S. Russell, G.M. Mutlu, G.R. Budinger, R. DasGupta, J. Varga, N. Kaminski, and C.J. Gottardi. 2014. Wnt coreceptor Lrp5 is a driver of idiopathic pulmonary

fibrosis. *Am. J. Respir. Crit. Care Med.* 190:185–195. http://dx.doi.org/10.1164/rccm.201401-0079OC

Landsman, L., and S. Jung. 2007. Lung macrophages serve as obligatory intermediate between blood monocytes and alveolar macrophages. *J. Immunol.* 179:3488–3494. http://dx.doi.org/10.4049/jimmunol.179.6.3488

Larson-Casey, J.L., J.S. Deshane, A.J. Ryan, V.J. Thannickal, and A.B. Carter. 2016. Macrophage Akt1 kinase-mediated mitophagy modulates apoptosis resistance and pulmonary fibrosis. *Immunity.* 44:582–596. http://dx.doi.org/10.1016/j.immuni.2016.01.001

Lavin, Y., D. Winter, R. Blecher-Gonen, E. David, H. Keren-Shaul, M. Merad, S. Jung, and I. Amit. 2014. Tissue-resident macrophage enhancer landscapes are shaped by the local microenvironment. *Cell.* 159:1312–1326. http://dx.doi.org/10.1016/j.cell.2014.11.018

Lavin, Y., A. Mortha, A. Rahman, and M. Merad. 2015. Regulation of macrophage development and function in peripheral tissues. *Nat. Rev. Immunol.* 15:731–744. http://dx.doi.org/10.1038/nri3920

Lawrence, M., W. Huber, H. Pagès, P. Aboyoun, M. Carlson, R. Gentleman, M.T. Morgan, and V.J. Carey. 2013. Software for computing and annotating genomic ranges. *PLOS Comput. Biol.* 9:e1003118. http://dx.doi.org/10.1371/journal.pcbi.1003118

Li, G.H., Y. Shi, Y. Chen, M. Sun, S. Sader, Y. Maekawa, S. Arab, F. Dawood, M. Chen, G. De Couto, et al. 2009. Gelsolin regulates cardiac remodeling after myocardial infarction through DNase I-mediated apoptosis. *Circ. Res.* 104:896–904. http://dx.doi.org/10.1161/CIRCRESAHA.108.172882

Lu, J.V., H.C. Chen, and C.M. Walsh. 2014. Necroptotic signaling in adaptive and innate immunity. *Semin. Cell Dev. Biol.* 35:33–39. http://dx.doi.org/10.1016/j.semcdb.2014.07.003

Lv, F.J., Y. Peng, F.L. Lim, Y. Sun, M. Lv, L. Zhou, H. Wang, Z. Zheng, K.M. Cheung, and V.Y. Leung. 2016. Matrix metalloproteinase 12 is an indicator of intervertebral disc degeneration co-expressed with fibrotic markers. *Osteoarthritis Cartilage.* 24:1826–1836. http://dx.doi.org/10.1016/j.joca.2016.05.012

Madala, S.K., J.T. Pesce, T.R. Ramalingam, M.S. Wilson, S. Minnicozzi, A.W. Cheever, R.W. Thompson, M.M. Mentink-Kane, and T.A. Wynn. 2010. Matrix metalloproteinase 12-deficiency augments extracellular matrix degrading metalloproteinases and attenuates IL-13-dependent fibrosis. *J. Immunol.* 184:3955–3963. http://dx.doi.org/10.4049/jimmunol.0903008

Marí, M., A. Tutusaus, P. García de Frutos, and A. Morales. 2016. Genetic and clinical data reinforce the role of GAS6 and TAM receptors in liver fibrosis. *J. Hepatol.* 64:983–984. http://dx.doi.org/10.1016/j.jhep.2015.11.042

Martinez, F.O., and S. Gordon. 2014. The M1 and M2 paradigm of macrophage activation: time for reassessment. *F1000Prime Rep.* 6:13. http://dx.doi.org/10.12703/P6-13

McCarthy, D.J., Y. Chen, and G.K. Smyth. 2012. Differential expression analysis of multifactor RNA-Seq experiments with respect to biological variation. *Nucleic Acids Res.* 40:4288–4297. http://dx.doi.org/10.1093/nar/gks042

Merad, M., M.G. Manz, H. Karsunky, A. Wagers, W. Peters, I. Charo, I.L. Weissman, J.G. Cyster, and E.G. Engleman. 2002. Langerhans cells renew in the skin throughout life under steady-state conditions. *Nat. Immunol.* 3:1135–1141. http://dx.doi.org/10.1038/ni852

Misharin, A.V., L. Morales-Nebreda, G.M. Mutlu, G.R. Budinger, and H. Perlman. 2013. Flow cytometric analysis of macrophages and dendritic cell subsets in the mouse lung. *Am. J. Respir. Cell Mol. Biol.* 49:503–510. http://dx.doi.org/10.1165/rcmb.2013-0086MA

Misharin, A.V., C.M. Cuda, R. Saber, J.D. Turner, A.K. Gierut, G.K. Haines III, S. Berdnikovs, A. Filer, A.R. Clark, C.D. Buckley, et al. 2014. Nonclassical Ly6C(-) monocytes drive the development of inflammatory arthritis in mice. *Cell Reports.* 9:591–604. http://dx.doi.org/10.1016/j.celrep.2014.09.032

Moore, B.B., R. Paine III, P.J. Christensen, T.A. Moore, S. Sitterding, R. Ngan, C.A. Wilke, W.A. Kuziel, and G.B. Toews. 2001. Protection from pulmonary fibrosis in the absence of CCR2 signaling. *J. Immunol.* 167:4368–4377. http://dx.doi.org/10.4049/jimmunol.167.8.4368

Moore, B.B., L. Murray, A. Das, C.A. Wilke, A.B. Herrygers, and G.B. Toews. 2006. The role of CCL12 in the recruitment of fibrocytes and lung fibrosis. *Am. J. Respir. Cell Mol. Biol.* 35:175–181. http://dx.doi.org/10.1165/rcmb.2005-0239OC

Morales-Nebreda, L., M. Chi, E. Lecuona, N.S. Chandel, L.A. Dada, K. Ridge, S. Soberanes, R. Nigdelioglu, J.I. Sznajder, G.M. Mutlu, et al. 2014. Intratracheal administration of influenza virus is superior to intranasal administration as a model of acute lung injury. *J. Virol. Methods.* 209:116–120. http://dx.doi.org/10.1016/j.jviromet.2014.09.004

Morales-Nebreda, L.I., M.R. Rogel, J.L. Eisenberg, K.J. Hamill, S. Soberanes, R. Nigdelioglu, M. Chi, T. Cho, K.A. Radigan, K.M. Ridge, et al. 2015. Lung-specific loss of α3 laminin worsens bleomycin-induced pulmonary fibrosis. *Am. J. Respir. Cell Mol. Biol.* 52:503–512. http://dx.doi.org/10.1165/rcmb.2014-0057OC

Moriwaki, K., S. Balaji, T. McQuade, N. Malhotra, J. Kang, and F.K. Chan. 2014. The necroptosis adaptor RIPK3 promotes injury-induced cytokine expression and tissue repair. *Immunity.* 41:567–578. http://dx.doi.org/10.1016/j.immuni.2014.09.016

Munger, J.S., X. Huang, H. Kawakatsu, M.J. Griffiths, S.L. Dalton, J. Wu, J.F. Pittet, N. Kaminski, C. Garat, M.A. Matthay, et al. 1999. A mechanism for regulating pulmonary inflammation and fibrosis: The integrin αvβ6 binds and activates latent TGF β1. *Cell.* 96:319–328. http://dx.doi.org/10.1016/S0092-8674(00)80545-0

Murray, L.A., R. Rosada, A.P. Moreira, A. Joshi, M.S. Kramer, D.P. Hesson, R.L. Argentieri, S. Mathai, M. Gulati, E.L. Herzog, and C.M. Hogaboam. 2010. Serum amyloid P therapeutically attenuates murine bleomycin-induced pulmonary fibrosis via its effects on macrophages. *PLoS One.* 5:e9683. http://dx.doi.org/10.1371/journal.pone.0009683

Murray, P.J., J.E. Allen, S.K. Biswas, E.A. Fisher, D.W. Gilroy, S. Goerdt, S. Gordon, J.A. Hamilton, L.B. Ivashkiv, T. Lawrence, et al. 2014. Macrophage activation and polarization: nomenclature and experimental guidelines. *Immunity.* 41:14–20. (published erratum appears in *Immunity*. 2014. http://dx.doi.org/10.1016/j.immuni.2014.07.009) http://dx.doi.org/10.1016/j.immuni.2014.06.008

Nahrendorf, M., and F.K. Swirski. 2016. Abandoning M1/M2 for a network model of macrophage function. *Circ. Res.* 119:414–417. http://dx.doi.org/10.1161/CIRCRESAHA.116.309194

Nakamura, A., R. Ebina-Shibuya, A. Itoh-Nakadai, A. Muto, H. Shima, D. Saigusa, J. Aoki, M. Ebina, T. Nukiwa, and K. Igarashi. 2013. Transcription repressor Bach2 is required for pulmonary surfactant homeostasis and alveolar macrophage function. *J. Exp. Med.* 210:2191–2204. http://dx.doi.org/10.1084/jem.20130028

Nayak, D.K., F. Zhou, M. Xu, J. Huang, M. Tsuji, R. Hachem, and T. Mohanakumar. 2016. Long-term persistence of donor alveolar macrophages in human lung transplant recipients that influences donor specific immune responses. *Am. J. Transplant.* 16:2300–2311. http://dx.doi.org/10.1111/ajt.13819

Nishikido, T., J. Oyama, A. Shiraki, H. Komoda, and K. Node. 2016. Deletion of apoptosis inhibitor of macrophage (AIM)/CD5L attenuates the inflammatory response and infarct size in acute myocardial infarction. *J. Am. Heart Assoc.* 5:e002863. http://dx.doi.org/10.1161/JAHA.115.002863

Oberst, A., C.P. Dillon, R. Weinlich, L.L. McCormick, P. Fitzgerald, C. Pop, R. Hakem, G.S. Salvesen, and D.R. Green. 2011. Catalytic activity of the caspase-8-FLIP(L) complex inhibits RIPK3-dependent necrosis. *Nature.* 471:363–367. http://dx.doi.org/10.1038/nature09852

Ostuni, R., V. Piccolo, I. Barozzi, S. Polletti, A. Termanini, S. Bonifacio, A. Curina, E. Prosperini, S. Ghisletti, and G. Natoli. 2013. Latent enhancers activated by stimulation in differentiated cells. *Cell.* 152:157–171. http://dx.doi.org/10.1016/j.cell.2012.12.018

Paul, F., Y. Arkin, A. Giladi, D.A. Jaitin, E. Kenigsberg, H. Keren-Shaul, D. Winter, D. Lara-Astiaso, M. Gury, A. Weiner, et al. 2015. Transcriptional heterogeneity and lineage commitment in myeloid progenitors. *Cell.* 163:1663–1677. (published erratum appears in *Cell.* 2016. http://dx.doi.org/10.1016/j.cell.2015.12.046) http://dx.doi.org/10.1016/j.cell.2015.11.013

Raghu, G., K.J. Anstrom, T.E. King Jr., J.A. Lasky, and F.J. Martinez. Idiopathic Pulmonary Fibrosis Clinical Research Network. 2012. Prednisone, azathioprine, and *N*-acetylcysteine for pulmonary fibrosis. *N. Engl. J. Med.* 366:1968–1977. http://dx.doi.org/10.1056/NEJMoa1113354

Riteau, N., P. Gasse, L. Fauconnier, A. Gombault, M. Couegnat, L. Fick, J. Kanellopoulos, V.F. Quesniaux, S. Marchand-Adam, B. Crestani, et al. 2010. Extracellular ATP is a danger signal activating P2X7 receptor in lung inflammation and fibrosis. *Am. J. Respir. Crit. Care Med.* 182:774–783. http://dx.doi.org/10.1164/rccm.201003-0359OC

Robinson, M.D., D.J. McCarthy, and G.K. Smyth. 2010. edgeR: A Bioconductor package for differential expression analysis of digital gene expression data. *Bioinformatics.* 26:139–140. http://dx.doi.org/10.1093/bioinformatics/btp616

Rock, J.R., C.E. Barkauskas, M.J. Cronce, Y. Xue, J.R. Harris, J. Liang, P.W. Noble, and B.L. Hogan. 2011. Multiple stromal populations contribute to pulmonary fibrosis without evidence for epithelial to mesenchymal transition. *Proc. Natl. Acad. Sci. USA.* 108:E1475–E1483. http://dx.doi.org/10.1073/pnas.1117988108

Salvesen, G.S., and C.M. Walsh. 2014. Functions of caspase 8: The identified and the mysterious. *Semin. Immunol.* 26:246–252. http://dx.doi.org/10.1016/j.smim.2014.03.005

Schneider, C., S.P. Nobs, M. Kurrer, H. Rehrauer, C. Thiele, and M. Kopf. 2014. Induction of the nuclear receptor PPAR-γ by the cytokine GM-CSF is critical for the differentiation of fetal monocytes into alveolar macrophages. *Nat. Immunol.* 15:1026–1037. http://dx.doi.org/10.1038/ni.3005

Scott, C.L., S. Henri, and M. Guilliams. 2014. Mononuclear phagocytes of the intestine, the skin, and the lung. *Immunol. Rev.* 262:9–24. http://dx.doi.org/10.1111/imr.12220

Seki, E., S. De Minicis, G.Y. Gwak, J. Kluwe, S. Inokuchi, C.A. Bursill, J.M. Llovet, D.A. Brenner, and R.F. Schwabe. 2009. CCR1 and CCR5 promote hepatic fibrosis in mice. *J. Clin. Invest.* 119:1858–1870. http://dx.doi.org/10.1172/JCI37444

Sennello, J.A., A.V. Misharin, A.S. Flozak, S. Berdnikovs, P. Cheresh, J. Varga, D.W. Kamp, G.R. Budinger, C.J. Gottardi, and A.P. Lam. 2017. Lrp5/β-catenin signaling controls lung macrophage differentiation and inhibits resolution of fibrosis. *Am. J. Respir. Cell Mol. Biol.* 56:191–201.

Shibata, T., U.B. Ismailoglu, N.A. Kittan, A.P. Moreira, A.L. Coelho, G.L. Chupp, S.L. Kunkel, N.W. Lukacs, and C.M. Hogaboam. 2014. Role of growth arrest-specific gene 6 in the development of fungal allergic airway disease in mice. *Am. J. Respir. Cell Mol. Biol.* 51:615–625. http://dx.doi.org/10.1165/rcmb.2014-0049OC

Sinadinos, A., C.N. Young, R. Al-Khalidi, A. Teti, P. Kalinski, S. Mohamad, L. Floriot, T. Henry, G. Tozzi, T. Jiang, et al. 2015. P2RX7 purinoceptor: A therapeutic target for ameliorating the symptoms of Duchenne muscular dystrophy. *PLoS Med.* 12:e1001888. http://dx.doi.org/10.1371/journal.pmed.1001888

Tan, C.D., C. Hobbs, M. Sameni, B.F. Sloane, M.J. Stutts, and R. Tarran. 2014. Cathepsin B contributes to Na+ hyperabsorption in cystic fibrosis airway epithelial cultures. *J. Physiol.* 592:5251–5268. http://dx.doi.org/10.1113/jphysiol.2013.267286

Toba, H., L.E. de Castro Brás, C.F. Baicu, M.R. Zile, M.L. Lindsey, and A.D. Bradshaw. 2016. Increased ADAMTS1 mediates SPARC-dependent collagen deposition in the aging myocardium. *Am. J. Physiol. Endocrinol. Metab.* 310:E1027–E1035. http://dx.doi.org/10.1152/ajpendo.00040.2016

van de Laar, L., W. Saelens, S. De Prijck, L. Martens, C.L. Scott, G. Van Isterdael, E. Hoffmann, R. Beyaert, Y. Saeys, B.N. Lambrecht, and M. Guilliams. 2016. Yolk sac macrophages, fetal liver, and adult monocytes can colonize an empty niche and develop into functional tissue-resident macrophages. *Immunity.* 44:755–768. http://dx.doi.org/10.1016/j.immuni.2016.02.017

Vlantis, K., A. Wullaert, A. Polykratis, V. Kondylis, M. Dannappel, R. Schwarzer, P. Welz, T. Corona, H. Walczak, F. Weih, et al. 2016. NEMO prevents RIP kinase 1-mediated epithelial cell death and chronic intestinal inflammation by NF-κB-dependent and -independent functions. *Immunity.* 44:553–567. http://dx.doi.org/10.1016/j.immuni.2016.02.020

Vuga, L.J., J.R. Tedrow, K.V. Pandit, J. Tan, D.J. Kass, J. Xue, D. Chandra, J.K. Leader, K.F. Gibson, N. Kaminski, et al. 2014. C-X-C motif chemokine 13 (CXCL13) is a prognostic biomarker of idiopathic pulmonary fibrosis. *Am. J. Respir. Crit. Care Med.* 189:966–974. http://dx.doi.org/10.1164/rccm.201309-1592OC

Wang, Z., M. Jinnin, Y. Kobayashi, H. Kudo, K. Inoue, W. Nakayama, N. Honda, K. Makino, I. Kajihara, T. Makino, et al. 2015. Mice overexpressing integrin αv in fibroblasts exhibit dermal thinning of the skin. *J. Dermatol. Sci.* 79:268–278. http://dx.doi.org/10.1016/j.jdermsci.2015.06.008

Wynn, T.A., and K.M. Vannella. 2016. Macrophages in tissue repair, regeneration, and fibrosis. *Immunity.* 44:450–462. http://dx.doi.org/10.1016/j.immuni.2016.02.015

Xue, J., S.V. Schmidt, J. Sander, A. Draffehn, W. Krebs, I. Quester, D. De Nardo, T.D. Gohel, M. Emde, L. Schmidleithner, et al. 2014. Transcriptome-based network analysis reveals a spectrum model of human macrophage activation. *Immunity.* 40:274–288. http://dx.doi.org/10.1016/j.immuni.2014.01.006

Yan, Y., L. Ma, X. Zhou, M. Ponnusamy, J. Tang, M.A. Zhuang, E. Tolbert, G. Bayliss, J. Bai, and S. Zhuang. 2016. Src inhibition blocks renal interstitial fibroblast activation and ameliorates renal fibrosis. *Kidney Int.* 89:68–81. http://dx.doi.org/10.1038/ki.2015.293

Yona, S., K.W. Kim, Y. Wolf, A. Mildner, D. Varol, M. Breker, D. Strauss-Ayali, S. Viukov, M. Guilliams, A. Misharin, et al. 2013. Fate mapping reveals origins and dynamics of monocytes and tissue macrophages under homeostasis. *Immunity.* 38:79–91. (published erratum appears in *Immunity.* 2013. http://dx.doi.org/10.1016/j.immuni.2013.05.008) http://dx.doi.org/10.1016/j.immuni.2012.12.001

Yu, Y.R., D.F. Hotten, Y. Malakhau, E. Volker, A.J. Ghio, P.W. Noble, M. Kraft, J.W. Hollingsworth, M.D. Gunn, and R.M. Tighe. 2016. Flow cytometric analysis of myeloid cells in human blood, bronchoalveolar lavage, and lung tissues. *Am. J. Respir. Cell Mol. Biol.* 54:13–24. http://dx.doi.org/10.1165/rcmb.2015-0146OC

Zhou, Y., H. Peng, H. Sun, X. Peng, C. Tang, Y. Gan, X. Chen, A. Mathur, B. Hu, M.D. Slade, et al. 2014. Chitinase 3-like 1 suppresses injury and promotes fibroproliferative responses in mammalian lung fibrosis. *Sci. Transl. Med.* 6:240ra76. http://dx.doi.org/10.1126/scitranslmed.3007096